



POLITECNICO DI TORINO

MECHANICAL ENGINEERING

Master course in Mechanical Engineering

Dynamics simulations of fretting wear for aero-engine applications

Supervisors:

Prof. Daniele Botto

Prof. Stefano Zucca

Candidate:

Luca Ciuffreda

244426 01/04/2020

Accademic Year 2019/2020

Torino - 01/04/2020

Acknowledgments

I would like to express my gratitude to my supervisors Prof. Danele Botto and Prof. Stefano Zucca who gave me the possibility to take part at this thesis project, and to my tutors Alfredo Fantetti and Lakshminarayana Reddy Tamatam who supported me during my thesis experience and were always available to give me useful advices. Thank you.

Abstract

A typical aircraft engine has many assemblies made up of thousands of contacts, such as blade tip shrouds and blade root joints. These contacts are employed to provide friction damping and vibration amplitude reduction at resonances. Contacts between components are a significant source of non-linearity due to the slip, stick and separation behavior during operation, which affect the structural response and the global dynamics of the engine. The tangential slip occurring at the interfaces leads to contact hysteresis and energy dissipation, thereby causing wear, which alters the contact behavior and change the dynamics. In particular, the aim of this study is to numerically predict of such contact parameters evolution during the wear process comparing the numerical results with the experimental one in order to validate the numerical models used to perform the analysis .

Summary

1	Introduction	5
1.1	Objectives	6
1.2	Outline of the Thesis	7
2	Literature Review	8
2.1	Finite Element Modelling	9
2.2	Component-Mode Synthesis - CB-CMS	11
2.3	Harmonic Balance Method	12
3	Description of the Test Case	13
4	Static Simulations - Finite Element Modelling of Fretting Wear	16
4.1	Description of the Numerical Code	16
4.1.1	Normal Contact Problem	16
4.1.2	Tangential Contact Problem	18
4.1.3	Masing Rule	19
4.2	Model used for the Static Simulations	20
4.3	Code Interface	28
4.4	Numerical Results	30
4.5	Experimental Results and Comparison	35
5	Nonlinear Dynamic Simulations of Fretting Wear	38
5.1	Description of the numerical model	38
5.1.1	Derivation of Nonlinear Friction Interface Elements	40
5.1.2	Modeling of the Nonlinear Interface Forces	41
5.2	Model Used for the Dynamic Simulations	42
5.3	Code Interface	46
5.3.1	Analysis controls	46
5.3.2	Linear Model Definition	49
5.3.3	Non Linear Model Definition	53

5.3.4	Output Requested	53
5.4	Numerical Results	54
5.5	Experimental Results and Comparison	58
6	Conclusions and Discussions	61

1 Introduction

Aircraft gas turbines are characterized by thousand of mechanical joints connecting components together. These joints introduce frictional contact because contact interfaces suffer from relative (sliding) motion due to vibration. Due to frictional contact the in service components are affected by wear that could dramatically change the interface and result in degraded performance or failure. Hence, it is of high importance to be able to accurately predict the effect of wear on the dynamics of the system. In order to predict wear, it is necessary to accurately model the contact, and this is done by means of the hysteresis loop. A typical hysteresis loop is shown in the fig. 1 and it is a plot of the friction force versus the relative displacement between two sliding contacts.

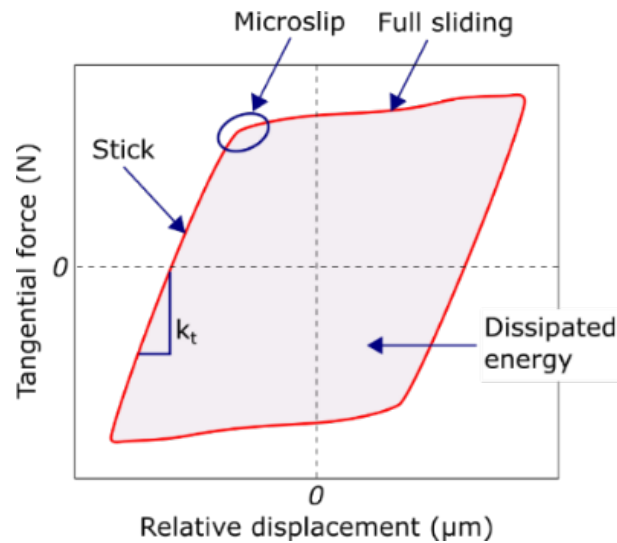


Figure 1: Typical hysteresis loop

From the hysteresis loop it is possible to extract the tangential contact stiffness from the slope of the stick portion and the friction coefficient from the sliding limit. These two parameters are given as input in numerical simulations in order to predict the nonlinear dynamics of structures with friction. The prediction of the dynamics of structures is very important in order to prevent failures. For this reason nonlinear dynamic modelling techniques were developed. Contact interfaces are modelled by several elements with relative nodes. Each pair of nodes of each surface in relative motion condition are linked with a normal and a tangential contact stiffness working in parallel. Predictive models to estimate tangential contact stiffness

and friction coefficient are needed to improve the accuracy of the simulations. However, good predictive models are missing in the literature due to a lack of physical understanding, which prevents the accurate modelling of these parameters. Botto and Lavella proposed a numerical method [3] to compute contact stiffnesses in quasi-static conditions using as input FE models. The routine from the Botto-Lavella study is used here to compute the contact stiffness of the specimen pairs used in the fretting rig. Specimens are discretized using a FE method and the contact area is finely meshed. Tangential forces and contact stiffness are computed from the code numerically, by giving as input the experimentally known parameters such as applied normal force and specimens' relative displacement at the contact. The routine also computes the evolution of hysteresis loops, normal pressure distribution, shear traction and slip distributions with progressing wear. For what concern the prediction of the non-linear dynamic behaviour of the structures the Vibration University Technological Center in Imperial College of London proposed a numerical method (FORSE) based on a multiharmonic representation for steady-state response and large-scale realistic friction interface modelling . The aim of this thesis is to use the two different numerical techniques to replicate the contact behaviour of sliding contacts and the dynamics behaviour of the structure undergoing such sliding contact.

1.1 Objectives

The objective of this thesis project is to perform static and dynamic simulations to replicate the behaviour of the friction rig built at Imperial College London. The test rig can perform high frequency fretting test in order to evaluate the dynamic friction contact parameters: friction coefficient μ and the tangential contact stiffness k_t . Experimental results have been provided as a benchmark to validate the numerical simulations. The latter have been performed according to static and dynamic conditions. A first set of static simulations, using the Botto-Lavella code, was run to investigate the effects of fretting wear on the evolution of the tangential contact stiffness and contact interfaces. A second set of dynamic simulations, using FORSE, was run to simulate the dynamic response of the friction rig undergoing fretting wear.

In particular, the following parameters have been obtained from simulations and compared to experiments:

- Hysteresis loops (and tangential contact stiffness) – from both static and dynamic simulations;
- Worn area of contact – from static simulations;
- Evolution of tangential contact stiffness with wear – from static simulations;
- Frequency response function – from dynamic simulations.

The obtained results have been compared to experimental results and provided insights on the reliability of the modelling approaches and on the physical origin of the contact phenomena.

1.2 Outline of the Thesis

This Master Thesis' work is organized as follow:

- Chapter 2 presents an overview of the physics of both friction coefficient and contact stiffness and the numerical approaches used to predict the fretting dynamics.
- Chapter 3 describes the friction rig of Imperial College, which provided the benchmark experiments used for the comparison, and has been modelled to be used in the numerical methods.
- Chapter 4 contains the description of the quasi-static numerical method developed in Politecnico di Torino [3] and the numerical results. The latter has been compared with the experimental results
- Chapter 5 includes an overview of the numerical method used to simulate the dynamics of the test rig. The numerical method, called FORSE, has been developed in Imperial College of London [7]. In chapter 5 the numerical results are presented and compared with the numerical ones.
- In Chapter 6 the main conclusions about the two type of numerical methods are presented with a short summary about the results.

2 Literature Review

This chapter provides a physical description of the main frictional parameters analysed and an overview of the numerical method used in this thesis. The research goal is to predict friction forces and energy dissipation at the contact interfaces because they strongly affect the dynamic behaviour of a system. In addition the energy dissipation in the contact interfaces produces wear and fretting fatigue phenomena that could lead to catastrophic failures of the jointed structures. The prediction of the dynamic response of jointed structures is not an easy problem to solve due to the poor understanding of the physics of friction.

Friction is the resistance that one surface or object encounters when moving over another. It occurs whenever relative sliding motion takes place between two surfaces and causes energy dissipation due to the force transmitted at the contact. The contact is a state of physical touching and it occurs when two bodies get in touch. Contact could happen in normal or tangential direction. Normal contact problems are well known and described in literature [12]. Tangential contact problems are more complicated due to the non linearity due to the presence of the friction. In order to get information about friction and consequently energy dissipation the major parameter used is the hysteresis loop. Hysteresis loop provide information on the macroscopic behaviour of two surfaces in contact. The information about the total amount of energy dissipated can be evaluated looking at the area limited by the loop. In a typical hysteresis loop shown in fig. 1, three contact regimes may occur, namely stick, microslip and full sliding conditions. The stick regime occurs when the friction force is less than the friction limit stated by the Amonton-Coulomb friction's law $T < \mu N$ where T is the friction force, μ is the friction coefficient and N is the normal load. When the contact interfaces are in stick regime the relation between sliding distance and tangential force is linear and the slope is k_t the tangential contact stiffness. The contact stiffness is a property of the contact interfaces and it is due to the elastic deformations of the asperities on the two surfaces in touching. The micro slip regime is due to the fact that some regions of the contact area are still in stick regime instead other regions are in sliding conditions hence when the tangential force overtake the friction limits. The full sliding regime is reached when in all the point of the contact area the sliding condition is reached. In order to predict all the main features of the contact interface

analytical and numerical methods has been used. Analytical methods are the fastest way to solve normal and tangential problems due to assumptions that simplified the two problems. The heavy simplification of the normal and tangential problems make the analytical method applicable only for few real simple cases. At the base of the analytical methods there is the Hertzian theory [10]. The Hertzian theory is referred to the frictionless contact between two elastic bodies under imposed normal loads. The numerical methods are able to solve normal and tangential problems of two contacting interfaces subjected to external forces. These methods are applicable to more general contact situations but due to the increasing complexity of the problem the numerical methods have some drawbacks linked to the numerical convergence of the solution and to high computational efforts. Numerical methods are divided into three major classes: Boundary Element Methods (BEM), Molecular Dynamics (MD) and Finite Element Methods (FEM). The latter has been used in this thesis in order to model the contact interface.

2.1 Finite Element Modelling

The FEM is a general discretization method for the solution of the partial derivative differential equations [9]. The finite element method consist on the subdivision of the volumes of a certain structure into finite elements and so into parts whose dimensions are not vanishingly small. Depending on the shape of the structure many type of elements have been formulated such as beam elements, shell elements, plate elements, solid elements. All these elements can be used to build the entire structure. The FEM is usually developed using matrix notation to obtain mathematical expressions easily readable by the computer codes. Each elements is characterized by specific points called nodes. Each nodes has a certain number of degrees of freedom (DOFs), in particular in the tridimensional space the number of DOFs for each node is usually three if the rotations are not considered. The DOFs of each elements are the displacement at given nodes. The displacement equation of the nodes inside each element is:

$$u(x, y, z, t) = N(x, y, z)q(t) \quad (1)$$

Where q is a vector where the n generalized coordinates of the element are listed and N is the matrix containing the shape functions. The shape functions are arbitrary but usually a set

of polynomials in the space coordinates are usually assumed [9]. In order to get the equation of motion of each element the stiffness and mass matrices must be stated. In order to get the stiffness and mass matrix a energy evaluation is used, in particular to get the stiffness matrix K the potential energy is evaluated instead the mass matrix M is evaluated starting from the kinetic energy:

$$U = \frac{1}{2} \int_V \epsilon^T \sigma dV = \frac{1}{2} q^T \left(\int_V B^T E B^T dV \right) q. \quad (2)$$

$$K = \int_V B^T E B dV \quad (3)$$

Where B is a matrix containing appropriate derivatives of the shape functions N and E is the Young modulus, this could varied along the x , y and z direction if the material is not isotropic. The recalling that u is the displacement vector the expression of the kinetic energy is:

$$T = \frac{1}{2} \int_V \rho \dot{u}^T \dot{u} dV = \frac{1}{2} \dot{q}^T \left(\int_V \rho N^T N dV \right) \dot{q}, \quad (4)$$

$$M = \int_V \rho N^T N dV \quad (5)$$

The equation of motion of the element is then the same of the discrete systems:

$$M \ddot{q} + K q = f(t) \quad (6)$$

Since a complex structure could be composed by thousands of elements with relative nodes, the matrices could be very large inducing high computational efforts. In order to reduce the computational time to reach the solutions some reduction techniques has been developed. The reduction techniques are used to reduce the number of the degree of freedoms without losing important information on the behaviour of the system reducing in this way the size of the model. For the reduction technique is necessary to chose slave degrees of freedom, dofs, to be linked to the master nodes solving the linear system finding out the expression of the slave dofs in function of the master ones. The reduction technique used in this thesis is the component-mode synthesis or Craig-Bampton Component Mode Synthesis (CB-CMS).

2.2 Component-Mode Synthesis - CB-CMS

The component-mode synthesis considers the slave dofs as constrained in this way neglecting their inertia contribution. The displacement vector of the constrained dofs x_2 is assumed to be equal to the sum of constrained modes x'_2 , hence the deformation pattern due to the displacement x_1 of the master dofs when no force is acting on them, plus the constrained natural modes x_2'' when the displacements of the master dofs x_1 are equal to zero. The expression of the constrained modes can be expressed in eq. 7 :

$$x'_2 = -K_{22}^{-1}K_{21}x_1 \quad (7)$$

The constrained normal modes can easily be computed by solving the eigenproblem stated in eq. 8 :

$$(-\omega^2 M_{22} + K_{22})x_2'' = 0 \quad (8)$$

Once the eigenproblem has been solved, the eigenvectors matrix Φ can be built:

$$x_2'' = \Phi \eta_2 \quad (9)$$

So that the generalized coordinates of the system can be written as:

$$\begin{Bmatrix} x_1 \\ x_2 \end{Bmatrix} = \begin{bmatrix} I & 0 \\ -K_{22}^{-1}K_{21} & \Phi \end{bmatrix} \begin{Bmatrix} x_1 \\ \eta_2 \end{Bmatrix} = \Psi \begin{Bmatrix} x_1 \\ \eta_2 \end{Bmatrix} \quad (10)$$

Even thou the number of modes is equal to the slave degrees of freedom the computational advantages grow together with the number of modes that can be neglected. From the eq. 10 is possible to get the transformation matrix Ψ that can be used to compute the new mass, stiffness, damping matrix and force vector [9].

2.3 Harmonic Balance Method

In order to solve the non linear dynamic behaviour of the test rig the harmonic balance method [4] has been used. Since in the case of study in this thesis is subjected to linear and non linear external forces its balance equation is:

$$M\ddot{Q} + C\dot{Q} + KQ = F_e + F_{NL}(Q, \dot{Q}) \quad (11)$$

Where M,C and K are the mass, damping and stiffness matrices of the system, Q is the degrees of freedom displacement vector, F_e is the external periodic forces vector and F_{NL} is the non linear forces vector. The harmonic balance method is used to evaluate the steady state response of the system subjected to non linear external forces. In particular since the external excitation is periodic also the displacements Q and the non linear forces would be periodic at steady-state. Hence they can be expressed as truncated of harmonic terms

$$Q = Q^{(0)} + \Re\left(\sum_{n=1}^{N_H} Q^n e^{in\omega t}\right) \quad (12)$$

$$F_E = F_E^{(0)} + \Re\left(\sum_{n=1}^{N_H} F_E^n e^{in\omega t}\right) \quad (13)$$

$$F_{NE} = F_{NE}^{(0)} + \Re\left(\sum_{n=1}^{N_H} F_{NE}^n e^{in\omega t}\right) \quad (14)$$

Where N_H is the maximum number of harmonics chosen and ω is the fundamental frequency of the excitation forces acting on the system. If the equations from 12 to 14 are replaced in the balance equation 11, a sets of complex algebraic equations are stated:

$$D^n Q^n = F_E^n + F_{NL}^n \quad (15)$$

where D^n is the n^{th} dynamic stiffness matrix of the system and its expression is:

$$D^n = -(n\omega)^2 M + in\omega C + K \quad (16)$$

The 0th order represents the static balance equation.

3 Description of the Test Case

The friction rig of Imperial College London [14] has been chosen as a test case to apply the numerical techniques for predicting the contact behaviour and the dynamic behaviour. Numerical results have then been compared with existing experimental measurements .

The aim of the experimental measurements is to get the main dynamic fretting parameters from the hysteresis loop such as: the friction coefficient μ , and the tangential contact stiffness K_t .

The principle of the friction contact parameter measurement is to provide a unidirectional relative sliding motion between two contact surfaces of two cylindrical specimens shown in fig 2.

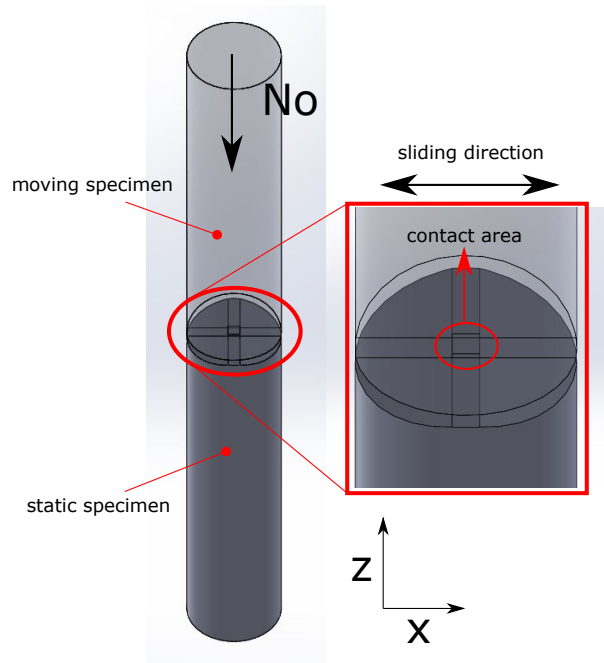


Figure 2: Cylindrical specimens

The specimen on the bottom is clamped to a static block instead the specimen on the top is clamped to a moving harm linked to a larger moving mass by several springs.The continuous contact between the specimens interfaces during the tests is ensured by applying a normal load N_0 by means of a pneumatic actuator placed on the top of the moving block (moving mass plus moving harm). The moving mass is exited by a shaker [14]. The benchmark experiments used

in this thesis were performed at 100 Hz harmonic excitation frequency instead the amplitude of the harmonic force produced F_{ex} has been changed for each test in order to evaluate how it could affect the system. In particular the F_{ex} amplitude, for a given normal load leads to different forced response functions (FRF) due to different contact area conditions:

- stick condition,
- stick/slip condition,
- full slip condition.

All these conditions are reflected on the relative displacement between the sliding specimens. This is measured slightly above and below the contact interfaces, less than 1mm far from the contact, by means of two Laser Doppler vibrometers (LDVs) fig 3. This accurate measurement method leads to a negligible effect of the bulk elastic deformation of the specimens, making the measurement of the tangential contact stiffness more reliable. The friction force is measured with dynamic load cells attached to the static block [1].

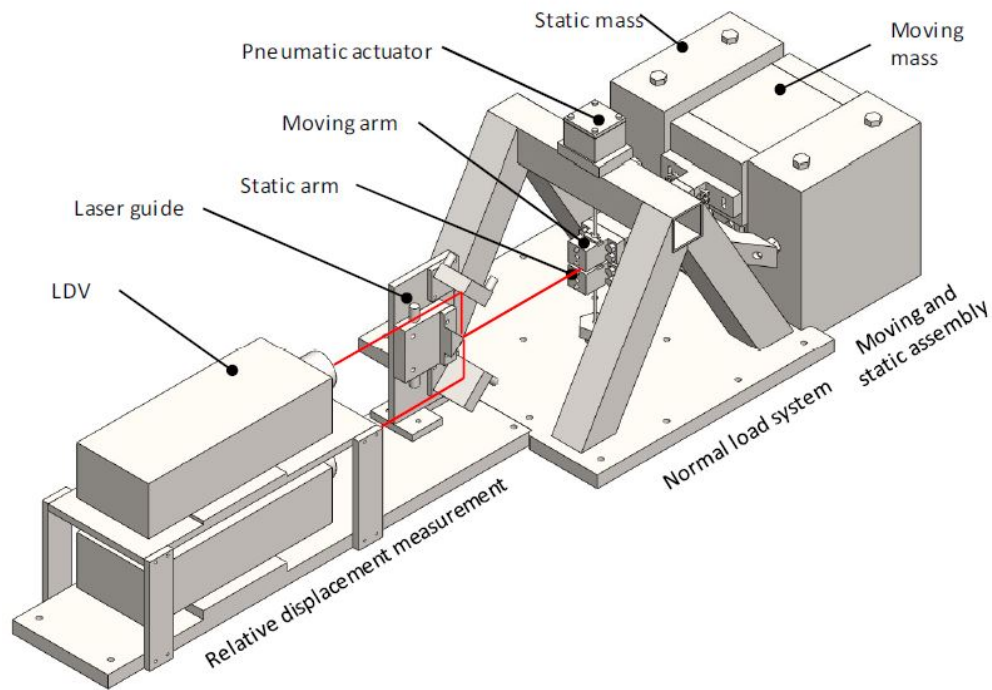


Figure 3: Test rig [14]

Measuring the relative displacement and the tangential force the hysteresis loop in fig. 1 can be depicted. The K_t is measured looking at the slope of the stick portion instead the friction coefficient from the limit value of the sliding condition. The limit value is given by a simple relation between the tangential F_t and normal force N_0 shown in eq. 17.

$$F_t = \mu N_0 \quad (17)$$

In order to get numerically what experimentally can be observed two type of numerical simulations have been performed:

- static simulations (needed to model fretting wear and hysteresis loops),
- dynamic simulations (needed to model FRFs and hysteresis loops).

4 Static Simulations - Finite Element Modelling of Fretting Wear

The goal of this chapter is to describe the numerical code developed at Politecnico di Torino to model the fretting wear [3]. The code simulates the fretting wear between two oscillating bodies in contact, and it evaluates pressure distribution, slip distribution, worn area and tangential force. From the tangential force distribution the code evaluates the total tangential force, and in relation with the tangential displacement, imposed by the user, the hysteresis loop is obtained for every wear cycle step. From hysteresis loops the tangential stiffness k_t is analysed in order to get its evolution versus cycles. The values of k_t are compared with the experimental results.

4.1 Description of the Numerical Code

This section describes the numerical code developed in [3]. In order to solve the contact problem, which is very complex in nature, the following assumptions are made to simplify the analysis :

- the material of the contact bodies (in this case the specimens) is linearly elastic, and the deformations are small,
- the roughness is neglected, and the contact surfaces are assumed perfectly smooth,
- An Amonton-Coulomb model of friction is used , this introduces three ideas: the force of friction is directly proportional to the applied normal load, the force of friction is independent of the apparent area of contact, Kinetic friction is independent of the sliding velocity. Moreover, the friction coefficient is constant.
- The normal and tangential contact problems are assumed uncoupled.

4.1.1 Normal Contact Problem

The normal contact problem refers to the computation of the contact area and the normal stress, or pressure distribution on two contacting interfaces subjected to a normal load. The

pressure distribution is replaced with discrete forces applied to the points of contact and the contact area is approximated with a set of points. At each iteration the true contact area must be evaluated because due to the wear it changes. According to this idea also the other parameters, like the pressure distribution, change. Numerically speaking the problem is to find out how many points are in or out the true contact area. At any of this points the first fundamental condition is that the sum of the separation between the bodies, the elastic displacement and the rigid body approach must be equal or greater than zero as stated in the eq. 18 [3]:

$$h(x, y) + (u_{1z} - u_{2z}) + e(\delta_{1n} - \delta_{2n}) > 0 \quad (18)$$

- $e = 0$ inside the contact area
- $e > 0$ outside the contact area

Where $h(x, y) = z_1 - z_2$ is the separation of the profiles in the undeformed state, u_z the elastic displacement along the vertical direction, and δ the rigid-body approach. The displacement along z in static can be related with the applied force according to eq. 19 :

$$Ku = f \quad (19)$$

Where K is the reduced stiffness matrix of the FE model of the specimen. The reduction can be performed with the Craig-Bampton method where the master nodes are those are lying on the contact surface and go under elastic deformation, and a set of distant nodes that define the normal rigid body approach. The distant nodes are used as a reference to determine the contact stiffness looking at their displacement on the tangential direction.

Until now only the normal contact problem is taken into account the tangential degree of freedom must be eliminated making it dependent of the normal dof as in eq. 20 :

$$\begin{bmatrix} K_{zz} & K_{zx} \\ K_{xz} & K_{xx} \end{bmatrix} \begin{Bmatrix} u_z \\ u_x \end{Bmatrix} = \begin{Bmatrix} f_z \\ f_x \end{Bmatrix} \quad (20)$$

$$u_x = K_{xx}^{-1}(f_x - K_{xz}u_z) \quad (21)$$

$$K_z u_z = f_z - K_{xx} K_{xz}^{-1} f_x \quad (22)$$

$$K_z = K_{zz} - K_{zx}K_{xx}^{-1}K_{xz} \quad (23)$$

According to the assumption that the normal contact is uncoupled from the tangential one the tangential force f_x is neglected, generally speaking the contact is friction less. Under this assumption the eq. 22 becomes:

$$K_z u_z = f_z \quad (24)$$

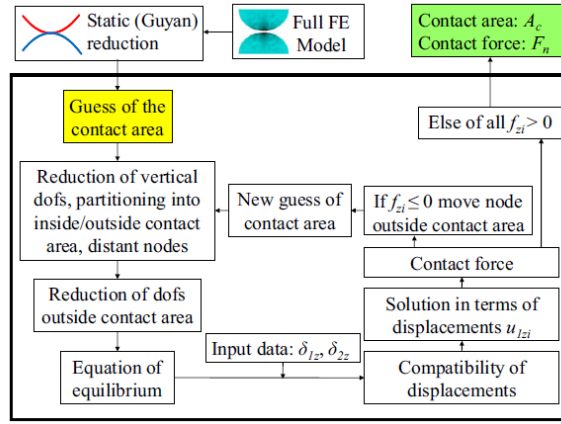


Figure 4: Flow chart of the procedure to solve the normal contact problem [3]

4.1.2 Tangential Contact Problem

Once the contact area has been determined the tangential contact problem is formulated assuming Coulomb's friction law.

$$\begin{bmatrix} K_{xx} & K_{xz} \\ K_{zx} & K_{zz} \end{bmatrix} \begin{Bmatrix} u_x \\ u_z \end{Bmatrix} = \begin{Bmatrix} f_x \\ f_z \end{Bmatrix} \quad (25)$$

$$u_z = K_{zz}^{-1}(f_z - K_{zx}u_x) \quad (26)$$

$$K_x u_x = f_x - K_{zz}K_{zx}^{-1}f_z \quad (27)$$

$$K_x = K_{xx} - K_{xz}K_{zz}^{-1}K_{zx} \quad (28)$$

Under the assumption that the normal and the tangential forces are uncoupled the force so that $f_x = 0$, the eq. 27:

$$K_x u_z = f_x \quad (29)$$

Solving the tangential contact problem the true contact area is split in different regions, namely adhesion region the one in which the nodal tangential force is less or equal of the nodal normal force times the friction coefficient $f_t < \mu f_n$, instead slip region where the tangential force is higher than the friction limit.

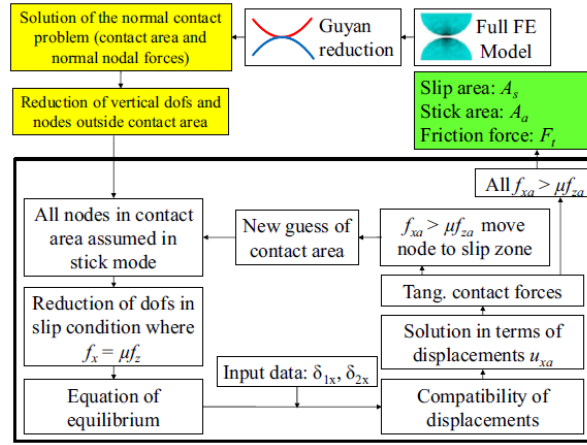


Figure 5: Flow chart of the procedure to solve the tangential contact problem [3]

4.1.3 Masing Rule

At this point the total tangential force can be evaluated summing all the nodal contributions. The relation between the tangential force and the rigid tangential displacement of the distant nodes gives the hysteresis loop. The latter is obtained by applying the Masing rule. In order to get the evolution of F_t in the micro slip regime, when the total tangential force is less than the friction limit, the so-called virgin-curve has been used. The virgin curve is the monotonic curve obtained increasing the tangential displacement up to the limit value μF_n , starting from the rest. The monotonic friction force f_m is a function of the virgin curve [3] [5]. The Masing assumption states that the unloading friction force is given by the friction force at the reversal F_t^{MAX} plus twice the monotonic force f_m evaluated for $\frac{(\delta_t - \delta_t^{MAX})}{2}$, namely [3]:

$$F_t = F_t^{MAX} + 2f_m\left(\frac{\delta_t - \delta_t^{MAX}}{2}\right) \quad (30)$$

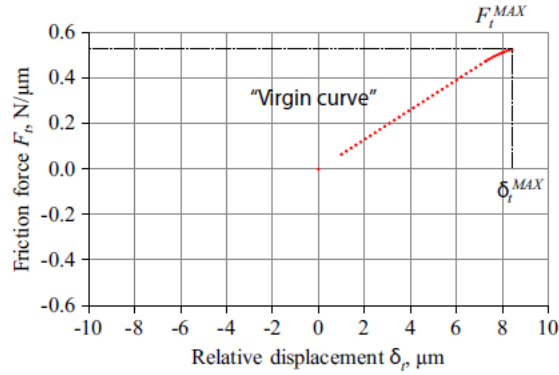


Figure 6: Example of virgin curve [3]

In order to get all the frictional parameters from the code, it needs of FE models where the contact areas are well defined. From the FE models the reduced stiffness and mass matrix of the two specimens are obtained in order to simulate the normal and the tangential behaviour. From the simulations the virgin curves for each cycle step are evaluated and applying the Masing rule also the hysteresis loops. From the hysteresis loops the tangential stiffness is calculated.

4.2 Model used for the Static Simulations

The goal of the numerical method is to simulate the evolution of the friction contact parameters by modelling the couple specimens used for the experiments on the friction rig of Imperial College. In order to analyse them in a numerical way the reduced stiffness and mass matrices of the body involved in the experimental test must be extrapolated. The method in which the two matrices were obtained is the FEM, using a software of finite element modelling such as Ansys. The idea is to model in the optimal way the contact interfaces between the two cylindrical specimens looking at their real features and then model them with the finite elements. The rig uses two cylindrical specimens, each of them has 8 mm diameter and it is 33 mm long. They have 1mm-wide rectangular surface. The specimens are rotated about their axis in order to make orthogonal the two flat rectangular surfaces generating a $1mm^2$ nominal contact area, as shown in fig. 2 . The contact area has been analysed with an electronic microscope finding out that, due to manufacturing, it has a curvature of: 1000 mm radius on the xz plane, 50

mm radius on the yz plane. These curvatures might have a strong effect on the numerical simulations, and for this reasons two FE models have been created one fully flat and one with curvature. The main sizes of the two specimens are reported in fig. 7.

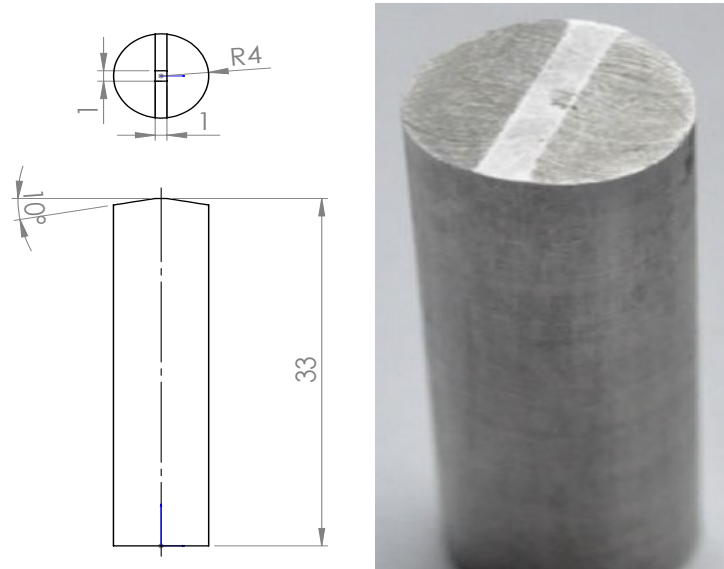


Figure 7: main dimensions of the specimen in mm

Starting from the main dimensions of the specimen a 3D model has been made using a commercial software : SolidWorks. In the 3D model the 1 mm^2 contact area was isolated making it such a stand alone volume for each specimen ,fig.8a,in order to be able to make a more precise element subdivision for the FEM. . In the end the assembly, as shown in fig. 8b, of the two bodies has been made and it has been exported as a parasolid file in Ansys.

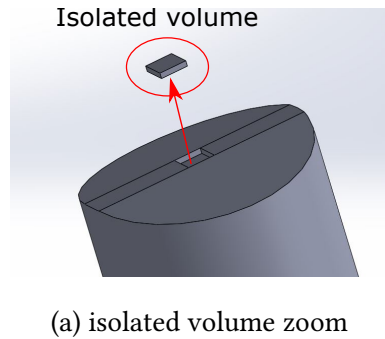


Figure 8: specimens 3D models

For the finite element modelling it is fundamental to declare the main characteristic of the material at first. The two specimen are made of steel with the following mechanical properties:

- Young modulus $E = 200000 \times 10^6 \left[\frac{N}{m^2} \right]$,
- density $\rho = 7800 \left[\frac{kg}{m^3} \right]$
- Poisson coefficient $\nu = 0.3$

Since ANSYS APDL haven' t got any unit of measure all the main physics dimensions must be consistent with the fundamental ones. Since the model was imported in mm and then scaled in μm all the mechanical properties have been converted according to the unit of measure adopted.

- Young modulus $E = 200000 \times 10^{-6} \left[\frac{N}{\mu m^2} \right]$,
- density $\rho = 7800 \times 10^{-24} \left[\frac{Mg}{\mu m^3} \right]$
- Poisson coefficient $\nu = 0.3$

After the material properties have been declared the element type must be chosen depending on the precision that the user wants for his analysis, but more precision means more computational time. For this study a simple brick element has been chosen with 8 nodes corresponding to the eight vertices of the cube (solid 185), fig.9 .

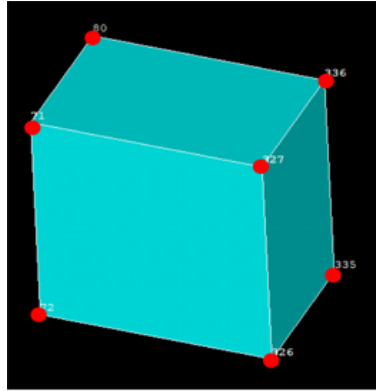
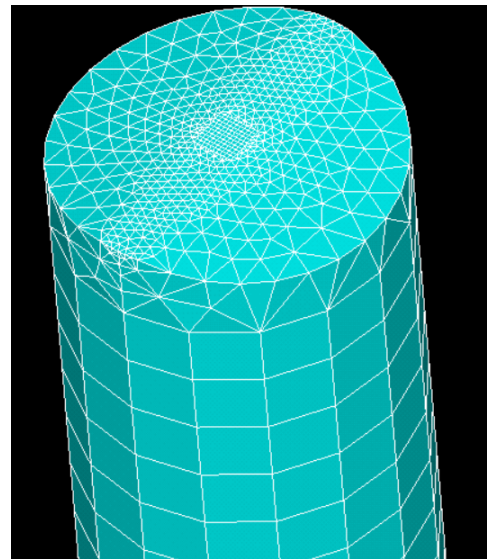


Figure 9: brick element with relative nodes

The mesh has been made differently according to the complexity of the volumes as shown in fig. 10, in particular the contact area has been subdivided in 10 by 10 elements (121 nodes).



(a) real specimen



(b) meshed model

Figure 10: comparison between modelled and real specimen

The same procedure has been made for the double curvature case but they are still difficult

to see also with a very high zoom on the interested area so ,after the mesh, the coordinates of the nodes that lie on it have been obtained and thanks to Matlab a better view has been realised, fig 11.

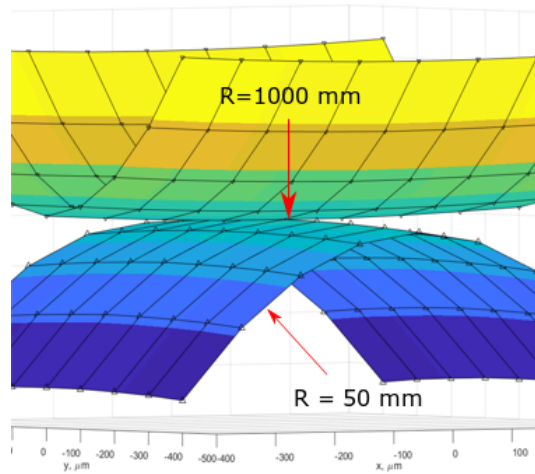


Figure 11: double curvature highlight

From the FE model it is possible to extract the stiffness, K , and mass, M , matrices of the two specimens, but since there are too many nodes the matrices would be very prohibitively needing large the computational time. In order to solve this problem a CB reduction method has been performed in order to get the reduced stiffness and mass matrices. The CB reduction method also known as component mode synthesis, it works partially with physical coordinates and partially with modal coordinates. The physical coordinates are related to the master nodes instead the modal coordinates are related to the slave nodes. It is very effective because not all the modes are necessary to the analysis introducing a further reduction in the computation. According to this concept 20 modes ranging beyond the operating frequencies have been chosen for the analysis. The master nodes, as stated in the section 4.1.1, have been divided into two sets: contact and distant nodes. The contact nodes lie on the contact area of 1 mm^2 instead the distant nodes lie on the circumference at the end of the specimen holders at 31 mm from the bottom as shown in fig. 12b :

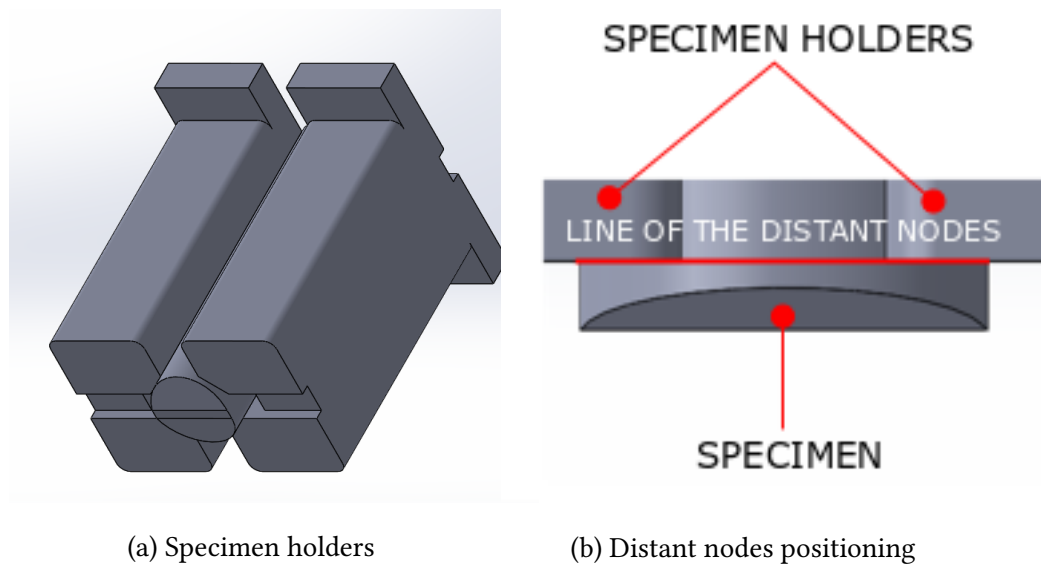


Figure 12: Specimen clamping

To have a better idea about the reduction a comparison between the specimens with all the relative nodes and the reduced model is shown in fig.13 :

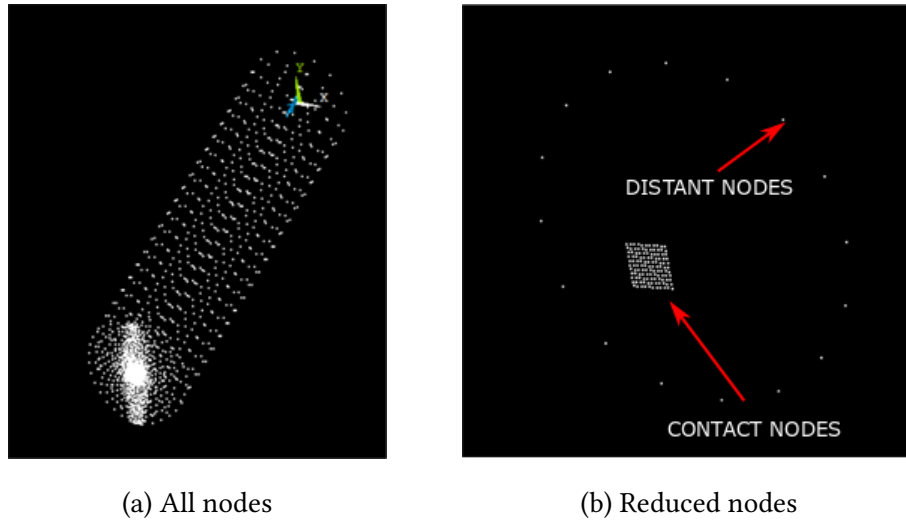


Figure 13: Comparison between the full model and the reduced one

The system passed from thousands of nodes to 121 contact nodes plus 16 distant nodes. Since each node has three degree of freedom the dimensions of the K and M matrices have been reduced at $(121 + 16) \cdot 3 + 20$ modes rows and columns, fig. 14.

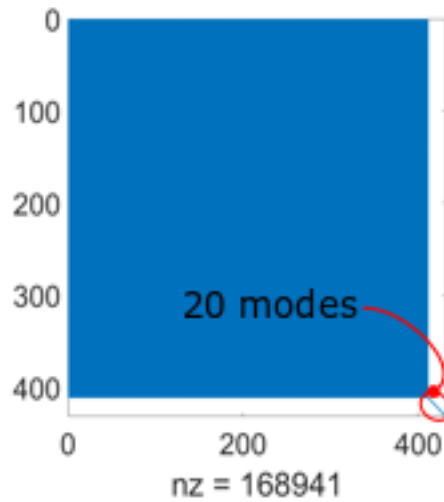


Figure 14: Matrix non zero elements

The reduction introduces some errors, so in order to verify how much is the amplitude of that a modal analysis has been performed for the two models getting the relative natural frequencies. The latter have been compared. Since the model has not boundary conditions the first six natural frequencies correspond to the six rigid body motions generally speaking their value is zero, the comparison up to the 12th frequency is shown in the tab. 1.

SET	FREQ. FULL MODEL [Hz]	FREQ. REDUCED MODEL [Hz]
7	29852	29874
8	29885	29907
9	47439	47489
10	69989	70228
11	70145	70379
12	76965	77207

Table 1: Frequencies for each model

The natural frequencies are quite close and hence the reduced model is verified.

4.3 Code Interface

In order to make the code works a certain number of inputs are needed. Looking at the two specimens, one is on the top, named body 1, and one is on the bottom, named body 2, contacting at the interface as shown in fig.15 .

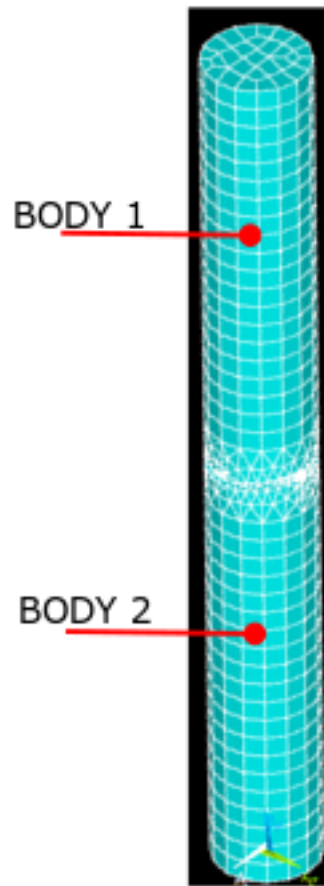


Figure 15: FEM specimens assembly

For each body the reduced stiffness and mass matrix has been evaluated with the CB reduction method. The degrees of freedom, dof, of the two matrices are ordered in growing order of number of nodes. The problem is that even if the numbering of the contact nodes is the same, the two specimens are tilted, as stated in section 4.2, this means that the nodal coordinates of the same node number are different. This is reflected also on the K and M matrices, so a re-ordering process is mandatory in order to couple the right nodes, in particular those have the same x and y coordinates. Keeping body 1 as reference the body 2 nodes have been reordered

in such a way their positions correspond to the nodes of the body 1 having the same x and y coordinates. From the new positioning the K and M matrices row and columns have been swapped. In addition to the K and M matrices the code needs others input listed in tab. 2:

INPUT MATRICES	
ProjectNameElements.mat	List of elements and relative nodes
ProjectNameKMbody1.mat	Stiffness and Mass matrices for body1...
ProjectNameKMbody2.mat	...and body2.
ProjectNameMasterNodesbody1.mat	Nodes list with coordinates for body1...
ProjectNameMasterNodesbody2.mat	...and body 2.

Table 2: Code inputs matrices

The element matrix is needed to evaluate the area of each element belongs to the contact interface. In this matrix is stored the node number of the element and the number of nodes belonging to each of them. The node number is needed in order to find the coordinates and in this way derive the element areas for each iteration. After giving to the code the necessary inputs the user can tune the simulations parameters that will be the conditions at which the two bodes are subjected. The simulation parameters are described in tab. 3:

SIMULATIONS PARAMETERS	
Normal force	Normal constant force FN In the contact ,in [N].
Delta Z1, Delta Z2	Vertical (z- direction) approaches between which the code looks for the normal force FN. Negative value parameters in μm
Stroke	Range of the tangential displacement in μm
Wear Cycle	Number of total wear cycles to be simulated
Cycles increment per stint	Number of cycles for which the contact geometry is assumed un- changed. If this increment is too large instability problem could arise in the simulation

Table 3: Code simulations parameters

At this point the code is ready to start the simulations but the user can choose also the output that he would like the code shows. The output chosen for this thesis are the ones listed in tab. 4

ANALYSED OUTPUT	
Worn geometry	Plot the geometry of the worn contact surfaces.
Pressure distribution	Plot the contact pressure in surf mode
Slip	Plot the slip between contact nodes in contour mode.
Tangential force	Plot the contact tangential force in contour mode.

Table 4: Outputs requested

The code computes the evolution of the contact interface at each wear iteration, and for each wear iteration the hysteresis loop is computed. The contact stiffness is extracted from every hysteresis loop so that its evolution versus wear can be studied and compared to the experiments.

4.4 Numerical Results

The simulations have been performed at first for the flat case and then for the curved one. The obtained results have been compared with the experimental ones in order to figure out which one of the two models describes better the fretting behaviour of the two specimens in terms of the Kt evolution respect to the number of cycles. The experimental tests have been performed according the following conditions :

- different normal load : 17 ,87 ,150 ,250 [N];
- tangential displacement : 14 μm ;
- friction coefficient μ : 0.88.

The output for the flat 17 N of normal load case are shown in fig. 16.

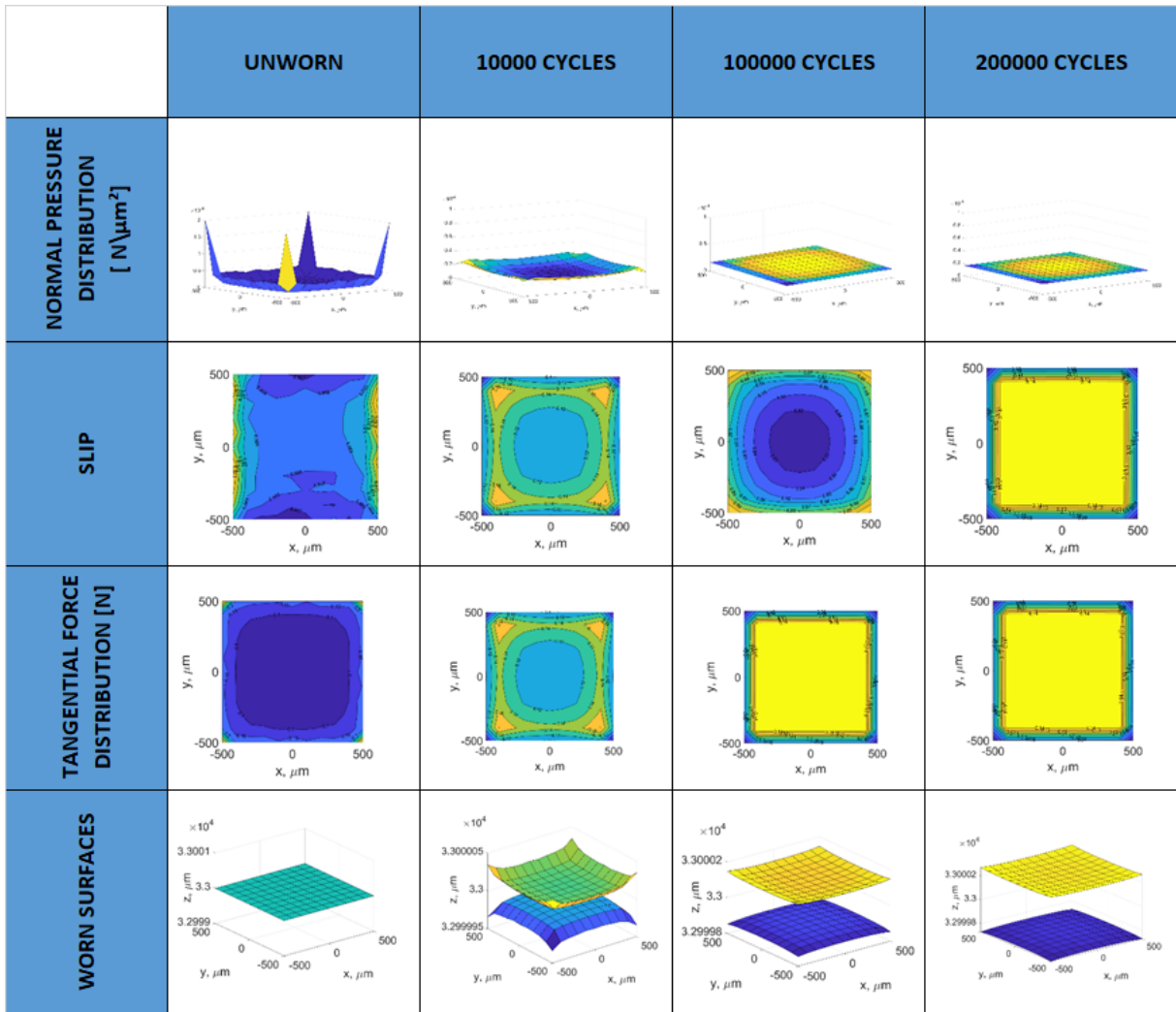


Figure 16: Flat contact area cycle conditions for 17 N normal load case

In particular the fig. 16 shows the evolution of the outputs, in tab. 9, requested for a certain number of cycles. The figure shows the evolution of normal pressure and the contact area increasing the number of wear cycles. In the beginning the pressure distribution is the typical one expected for a flat-on-flat contact [11], and then it tends towards a constant pressure distribution which is reached after about 30,000 cycles. The area of contact decreases with wear because in the beginning the contact is flat-on-flat and hence all the interface is in full contact, and towards the end it becomes similar to a spherical contact due to increased wear at the edges, and hence the real area of contact decreases. Fig. 17 shows the evolution of the contact stiffness with the wear cycles, in order to compare it with the experimental results.

Unfortunately, the simulation shows that the contact stiffness slightly decreases with wear on the contrary of what has been shown by the experimental results. The numerical results are acceptable since the area of contact in the simulation decreases with wear as shown in Fig. 16, thus resulting in a lower final contact stiffness.

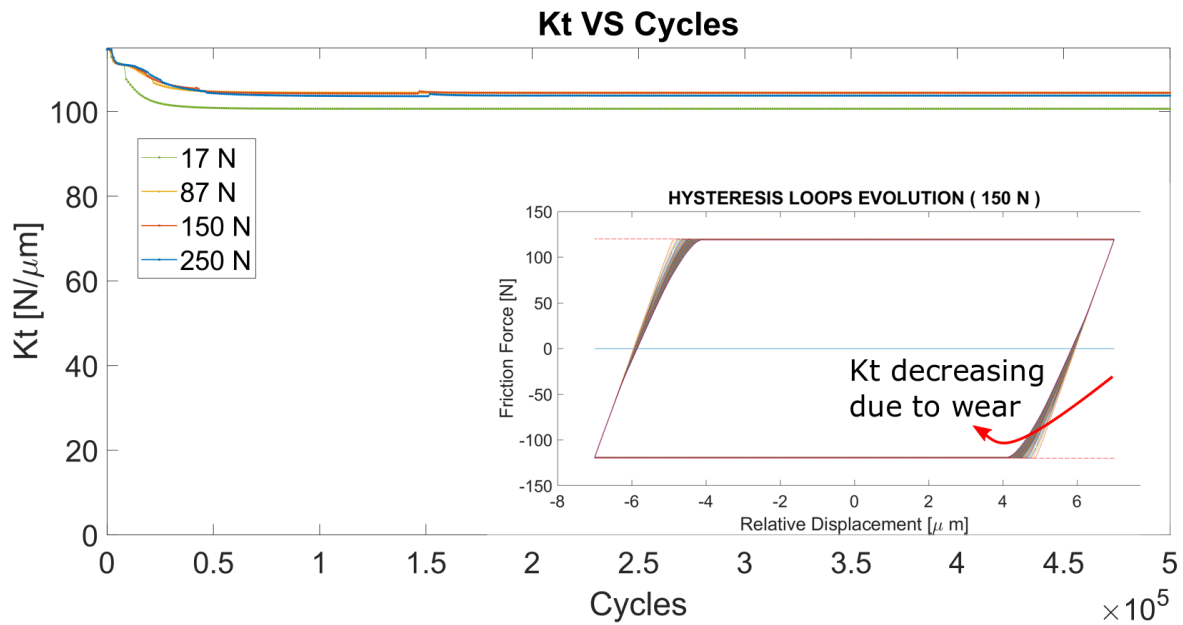


Figure 17: Kt versus number of cycles (Flat case)

At this point the more realistic FE model of the specimens has been analysed, the curved one previously shown in fig 11. The slight curvatures and the fact that specimens are rotated, results in a sphere on sphere equivalent contact. Due to the curvatures, the contact in the beginning is only on a point and the contact area gradually increases with wear as shown in fig. 18.

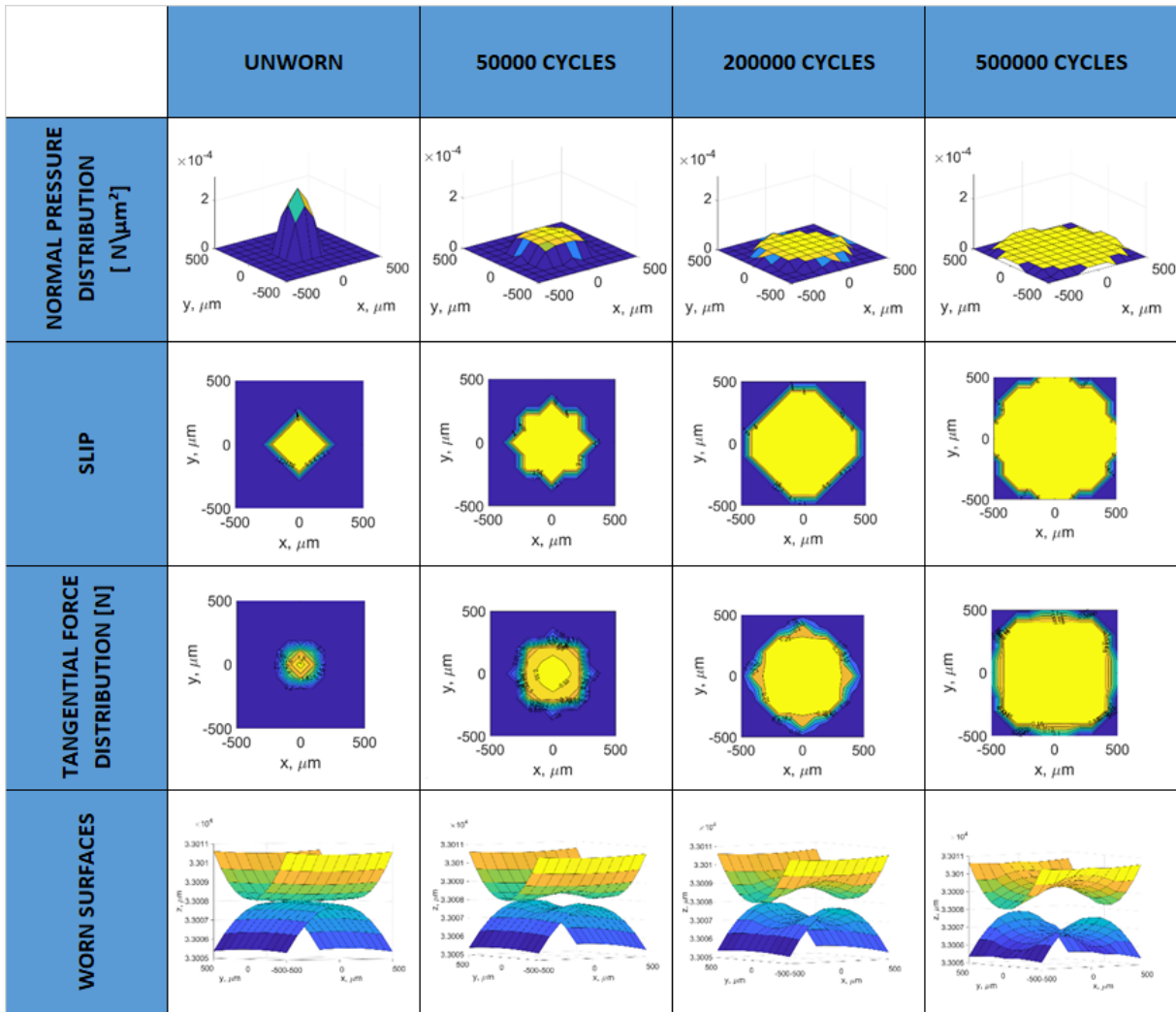


Figure 18: Contact area conditions for different number of cycles, 17 N normal load (Curved case)

This increase in the contact area results in an increase in the contact stiffness. The evolution of the contact stiffness with wear cycles is shown in Fig. 19 .

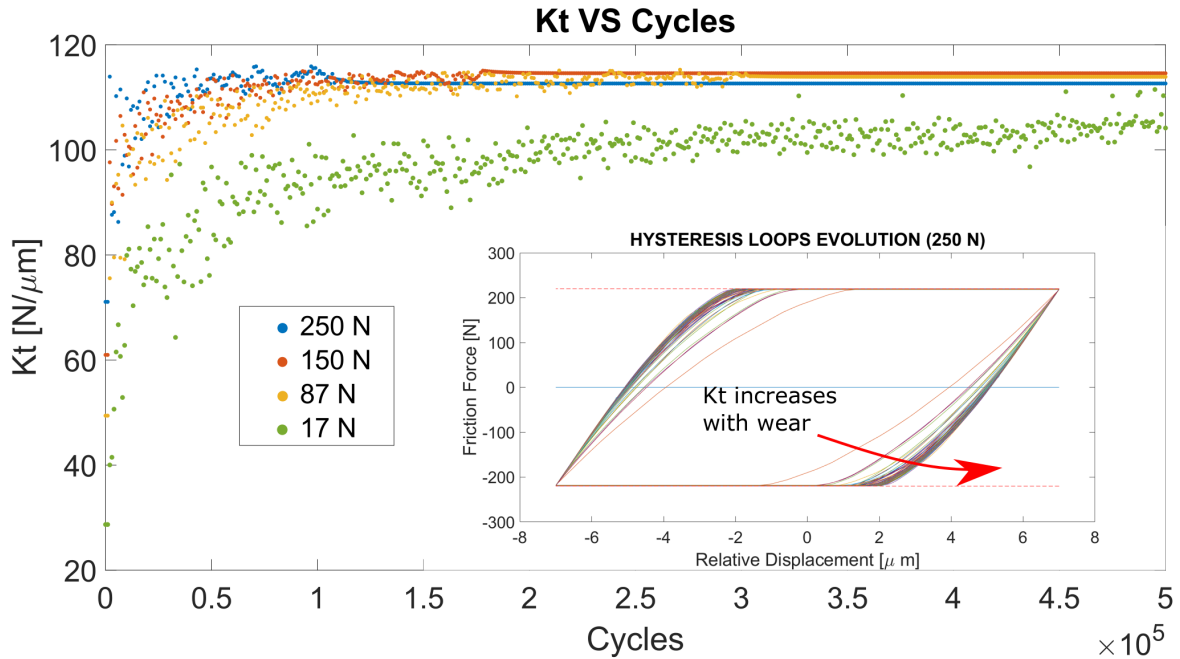


Figure 19: K_t versus number of cycles (Curved case)

It can be noticed that a certain point the curves of the 87, 150 and 250 N normal load become flat reaching the steady state condition within 500000 wear cycles, in which the 17 N normal load case never reach the steady state condition. Physically the steady state condition is reached due to a full steady interaction between the contact interfaces. These interactions increase the resistance to motion resulting in increasing of the contact stiffness [8]. From literature [1] it is suggested to plot the evolution of the contact parameters versus the cumulative energy dissipated as shown in fig. 20 rather than fretting cycles, since the cumulative energy dissipated allows for a more reliable comparison of results obtained in different test conditions. The cumulative energy dissipated is obtained as the cumulative sum of the energy dissipated for each cycle.

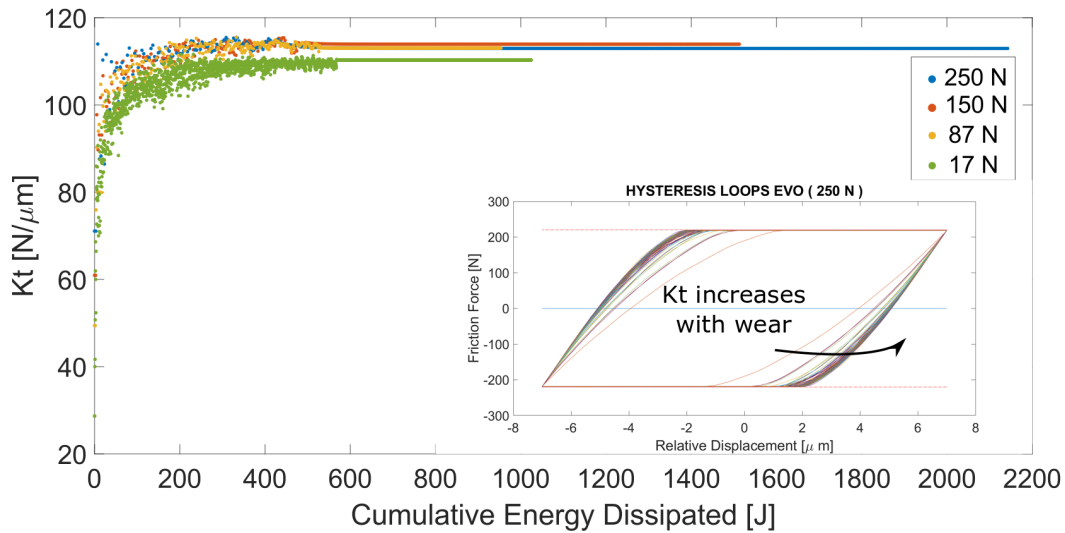


Figure 20: Kt versus cumulative energy dissipated

In fig. 20 the 87,150 and 250 N normal load cases have been submitted to the same number of fretting cycles. In particular can be noticed that the steady state condition occurs in the same point but the final value of cumulative energy dissipation is different. In particular higher is the amplitude of the normal load and higher is the energy dissipated. This result is in accordance with the physical evidence because increasing the normal load, the friction limit is higher and so in the same conditions of sliding distance, the area limited by the hysteresis loop generated increases. For the 17 N normal load case 2500000 wear cycles have been performed in order to reach the steady state conditions, confirming the idea that the normal load affect the amount of energy dissipated. Once the numerical results have been obtained, they were compared with experimental measurements in order to validate or not the two models: flat and curved.

4.5 Experimental Results and Comparison

The experimental analysis [1] were conducted in Imperial College of London using the in-house test rig described in section 3. The test rig is used to measure the relative displacements of two sliding specimens and the friction force . By measuring the tangential displacement and the tangential force it is possible to get the hysteresis loop. From the hysteresis loop the frictional parameters, such as friction coefficient and contact stiffness, can be extracted. These frictional parameters have been extracted as functions of energy dissipated. Several

fretting tests were conducted over different time spans in order to capture the evolution of the hysteresis loops with wear. The numerical simulations conditions are:

- constant normal load $F_n = 60N$;
- excitation frequency $f = 100Hz$;
- nominal area of contact $1mm^2$;
- specimens material = stainless steel;
- temperature = $25\text{ }C^o$

All the tests have been conducted at imposed later forces that generated different strokes characterized by an average of $14\mu m$ and $22\mu m$ sliding distances. One of the main differences with the numerical simulations is that in experimental tests the sliding distances is not imposed but it is a function of time-dependent coefficient of friction and contact stiffness in reaction to an external periodic excitation. The experimental results are shown in fig. 21.

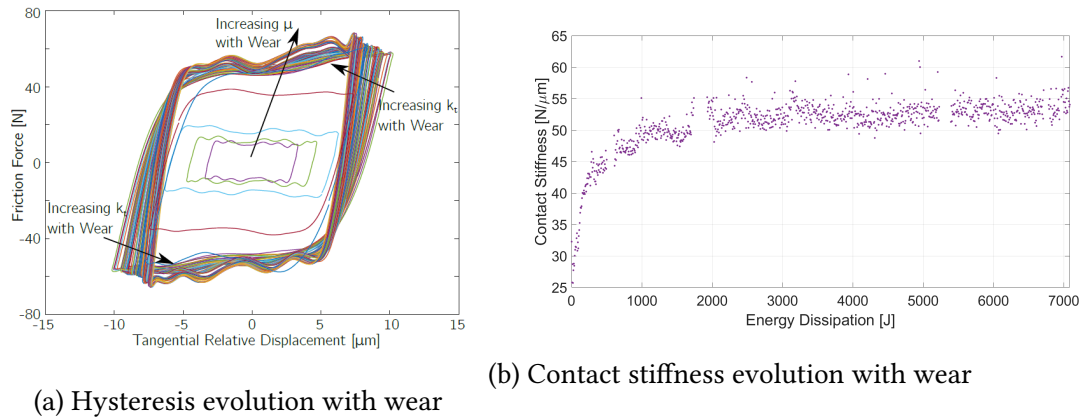


Figure 21: Experimental results

From fig. 21 it possible to get some conclusions. It is clear that the contact stiffness increases with wear, as shown in fig. 21b, because the slope of the stick portion in the hysteresis loops increases as well, as shown in fig. 21a, starting from an initial value of $26\frac{N}{\mu m}$ and reaching a steady state value of about $50\frac{N}{\mu m}$. This trend is physically due to:

- an increased conformity of the contact surfaces;

- the increased interaction between the wear grooves;

The increase in the interface conformity leads to a larger amount of asperities in contact, which in turn contributes to the increase in the contact stiffness. The increase in the interaction between wear grooves is due to the conformity of peaks and valleys, which lock the surfaces together and add elastic resistance to the relative motion during the stick phase [8]. The results in fig. 20 are quite promising as they are in accordance with the experimental trend, and also the values are of the similar order of magnitude. The difference in values could be due to the fact that the FE model has a perfectly smooth contact interface, while the real specimens have a roughness. However it is demonstrated that the curvatures affect strongly the numerical results bringing out that the ones obtained for the flat on flat contact, fig. 17 are not in conformity to what experimentally is measured.

5 Nonlinear Dynamic Simulations of Fretting Wear

The simulations of the non-linear dynamics of the test rig have been performed using the non-linear structural dynamic analysis code FORSE developed in Imperial College of London for Rolls-Royce [2][7]. It is based on a multiharmonic representation for steady-state response and large-scale realistic friction interface modelling of the two specimens. The code requires as input the modal shapes of the two bodies obtained from a finite element commercial software Abaqus and an accurate contact interface description, in particular the pair of nodes in contact between the two bodies must be defined. Each pair of contact nodes is linked by contact interface elements, used to describe the dynamic role of the roughness in the response of the entire system, what was missing in the quasi-static simulations. The parameters required in the non linear analysis can be separated into three main groups:

- the friction interface parameters that describe the material properties of contact area
- the modelling parameters that define the nonlinear model and its excitation,
- the analysis parameters, which control the accuracy and speed of calculations. [13]

Furthermore the simulations gives as results also the nodal conditions (full separation, stick, stick/slip or slip condition) for each frequency.

5.1 Description of the numerical model

The numerical approach used in FORSE (FORced Response Suite) to analyse the non-linear system of the test rig is based on the multi-harmonic representation of the steady-state response. The equation of motion 31 of the moved specimen consist of a linear part, which is independent of the vibration amplitudes, and a non linear part resulting from friction at the contact area interface:

$$M\ddot{q}(t) + C\dot{q}(t) + Kq(t) + f[q(t), \dot{q}(t)] = p(t) \quad (31)$$

Where M, C and K are the mass, damping and stiffness matrices, $q(t)$ is the contact nodes dofs vector and $f[q(t), \dot{q}(t)]$ is a vector of nonlinear, friction interface forces, which is dependent

on displacements and velocities of the interacting nodes, and $p(t)$ is the vector of the external exiting forces. By applying the Harmonic Balance Method is possible to solve the non linear equations by a set of non-linear algebraic equations. This is possible because the external force $F_e x$ is periodic. If the external force is periodic also the displacements and the non-linear forces would be periodic. They can be approximated by Fourier series as:

$$q(t) = Q_0 + \sum_{j=1}^n (Q_j^c \cos(m_j \omega t) + Q_j^s \sin(m_j \omega t)) \quad (32)$$

Where Q_j^{cs} are the vectors of the harmonics coefficient respectively of the cosine and sine parts instead n is the number of harmonics needed to describe the variation of the physical dimensions in time , higher is n higher is the precision but heavier computational speaking. The flow chart of the main computational processes performed by the code is shown in fig. 22.

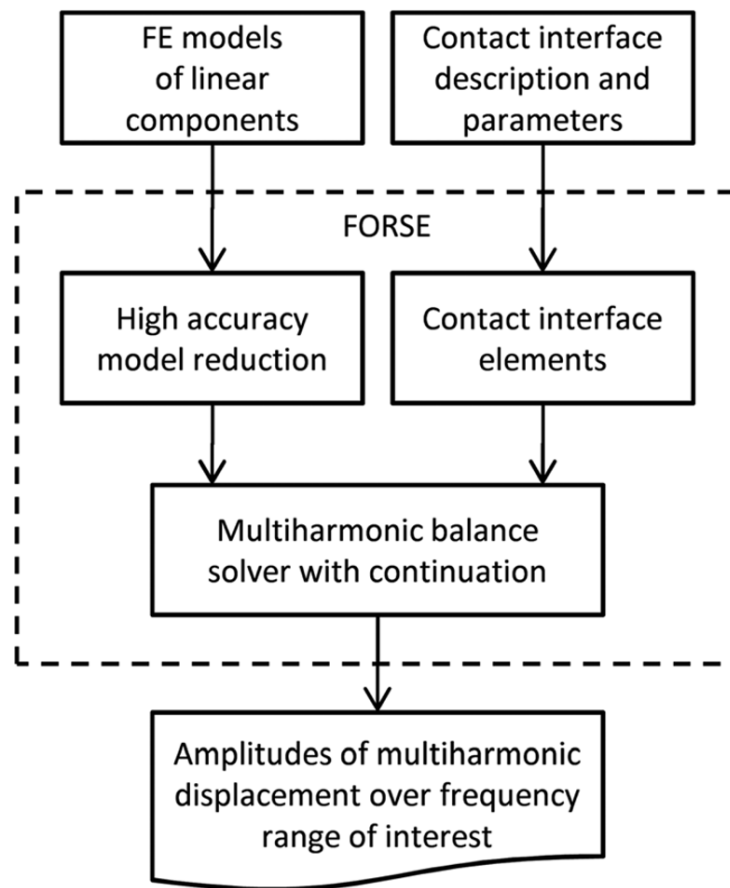


Figure 22: Computational flow chart [2]

5.1.1 Derivation of Nonlinear Friction Interface Elements

The roughness of the contact interface is modelled by non linear friction interface elements. This elements are characterised by specific mechanical properties, as shown in fig. 23:

- friction coefficients μ in order to link normal load F_{z0} with tangential forces f_x ;
- tangential stiffness k_x or k_t directed along the tangential motion direction;
- normal stiffness k_z or k_n directed along the normal direction;
- the initial gap g between the pair of contact nodes linked by the friction interface elements.

The initial gap depends on the magnitude of the static normal load , higher is the normal load less is the initial gap between the nodes, defining the initial conditions of the non linear simulations.

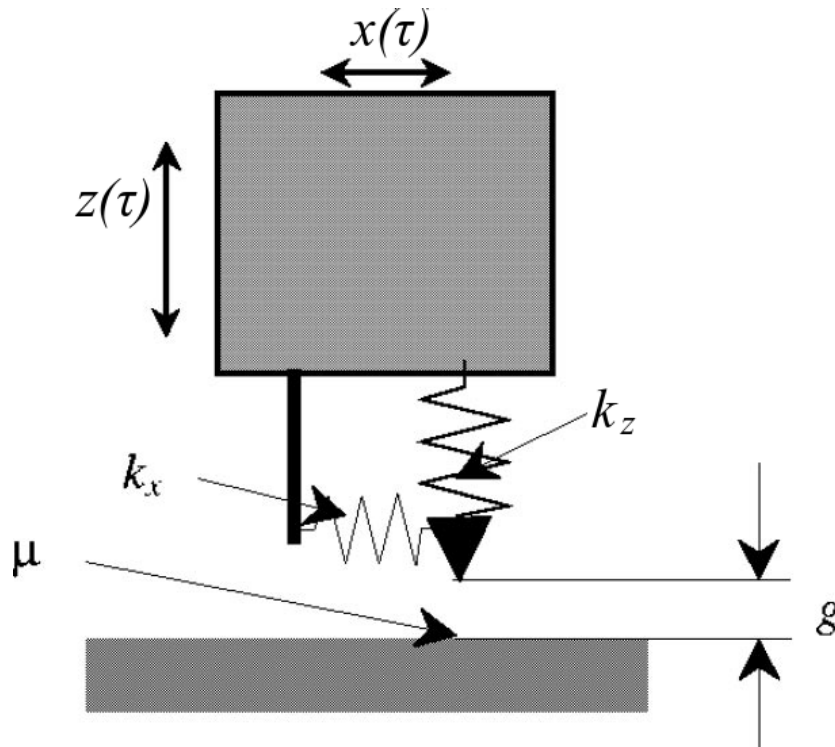


Figure 23: Interface element [7]

To derive the expression for friction interface matrices, the relative motion of the contact nodes in terms of tangential, x , and normal, z , must be taken into account. The periodic motion

of each nodal degree of freedom can be represented by a sum of all harmonic components analyzed as stated in eq.33 :

$$x(\tau) = H_{(\tau)}^T X; \quad z(\tau) = H_{(\tau)}^T Z \quad (33)$$

Where τ is the non dimensional period of time, $\tau = \omega t$, X and Z are the vectors containing the harmonic coefficients of the relative motions; H is the vector composed by harmonics functions, which is used for transition from frequency to time domain [7].

5.1.2 Modeling of the Nonlinear Interface Forces

During the relative motions between the contact nodes several states could happen. The motion along the normal direction determines if the nodes are in contact or they are separated. During contact other two possible conditions could happen: stick or slip condition. In the slip condition the tangential force f_x , is a dry friction force, instead in the stick condition f_x is determined by the elastic deformations of the asperities. Expressions for non linear interaction forces can be derived for all possible states in the following form:

Tangential force:

$$f_x = \begin{cases} f_x^0 + k_x(x - x_0) & \text{for stick,} \\ \xi \mu f_y & \text{for slip,} \\ 0 & \text{for separation} \end{cases} \quad (34)$$

Normal force :

$$f_z = \begin{cases} F_{z0} + k_z z & \text{for contact,} \\ 0 & \text{for separation} \end{cases} \quad (35)$$

ξ is the sign function in case of constant normal load determined by the tangential velocity $\xi = \text{sgn}(\dot{x}(\tau_{slip}))$ where τ_{slip} is the time instant of slip state initiation. The other constants in eq. 34 and 35, $x_0 = x(\tau_{stick})$ and $f_x^0 = f_x(\tau_{stick})$ are values of the relative tangential displacement and the interaction force at the beginning of the stick-state, τ_{stick} , respectively.

5.2 Model Used for the Dynamic Simulations

The two specimens was modelled as in the static simulations, section 4, using the commercial software Abaqus. In order to simplify the model, for the dynamic simulations the major curvature of 1000 mm has been neglected. The two specimens have the same disposition used for the static simulations but there is a difference: in the dynamic simulations the contribution of the test rig has been implemented. The test rig was modelled with a 2 degrees of freedom lumped parameters model where the main features are shown in fig. 24.

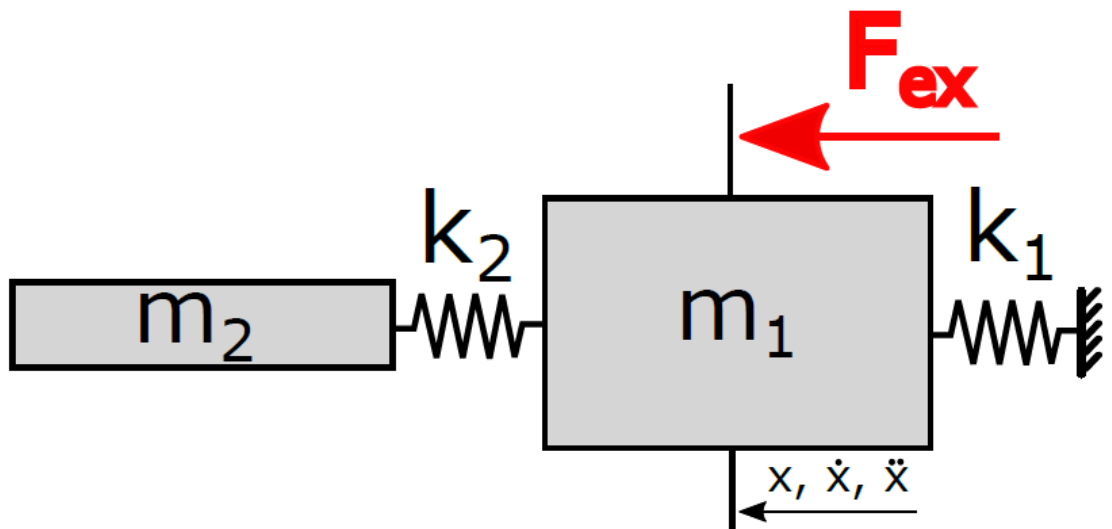


Figure 24: 2DOF lumped parameters model [8]

Where k_1 is the leaf spring, m_1 is the moving mass, k_2 is the connecting spring stiffness, m_2 is the moving harm mass. To better understand the meaning of the lumped parameters in the 2 DOFs model the complete system is shown in fig. 25, where is more clear where the external periodic force F_{ex} is applied by a shaker.

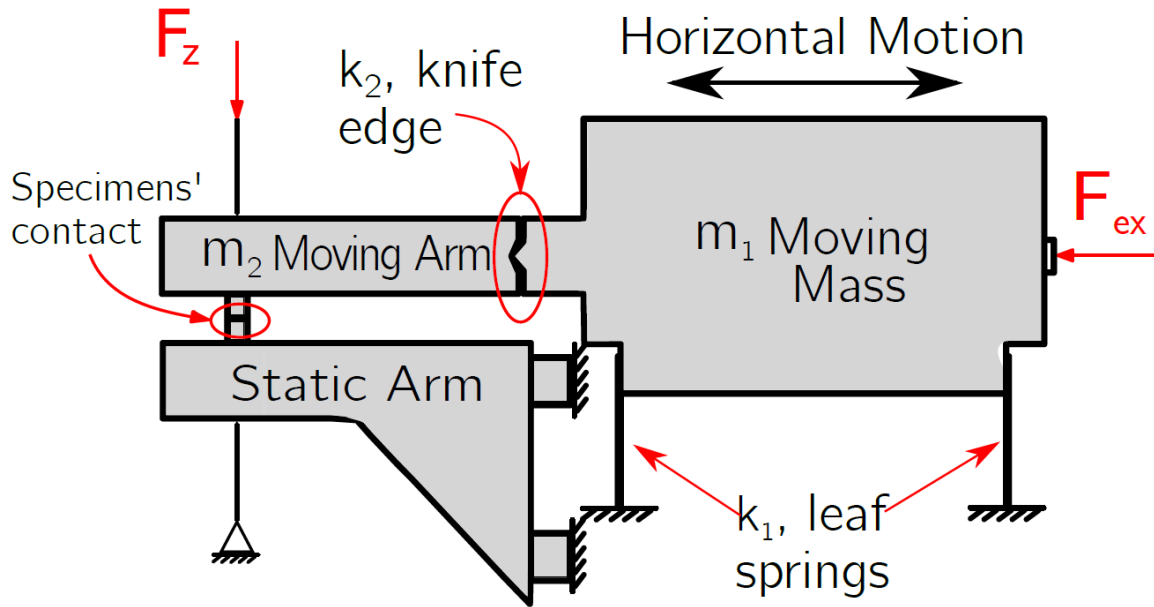


Figure 25: Complete system [1]

In the end two subsystems must be modelled in order to get their modal shapes useful for the dynamic simulations:

- 2DOF implemented to the body 1;
- body 2.

Before the implementation of the 2DOF system, the two specimens must be modelled. As for the static simulations, a stand alone volume that contain the contact area has been created in order to better mesh the friction interface. After the model mesh two reference points (RP1 and RP2 in fig. 26) have been created in order to attach the two lumped masses $m_1 = 21.152Kg$ and $m_2 = 1.189Kg$. The two lumped masses are linked by the connecting spring having stiffness $k_2 = 273 \cdot 10^3 \frac{N}{mm}$. The moving mass m_2 is linked to the ground by the leaf spring having stiffness $k_1 = 1.3469 \cdot 10^3 \frac{N}{mm}$. Looking at the test rig the two lumped masses have been constrained to move only on the x tangential direction and z normal direction like the specimen. The latter is linked to the 2DOF system by a rigid beam interaction between the nodes that lie on the clamped part surface and m_2 . At this point the system would have a not constrained degree of freedom, the normal one. In order to avoid any rigid body motion

on the z direction a dummy spring having a very little stiffness $k_d = 10^{-6} \frac{N}{mm}$ acting on the normal direction has been added. The rigid body motion must be avoided because of numerical problem with the code.

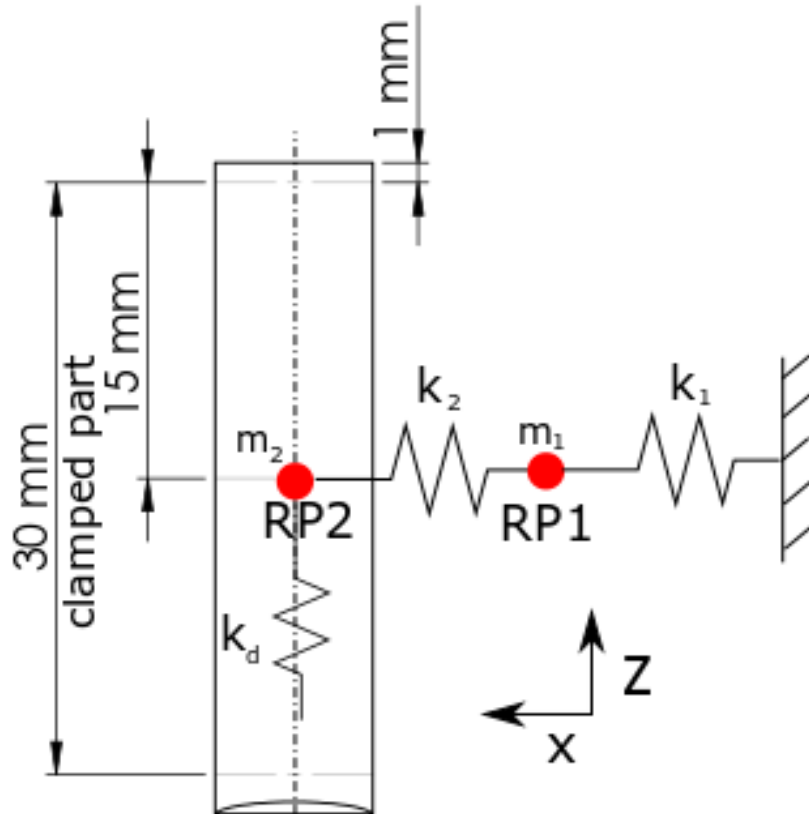


Figure 26: Implementation of the 2DOF model

For what concern the fixed specimen (body 2) a reference point RP3 has been created. The fixed specimen is clamped like the moving specimen and so the nodes that lie on the surface of the clamped part are linked to the reference point like in body 1 but the reference point RP3 is fully constrained. At this point the modal analysis for the two bodies has been performed getting as output the modal shapes of a certain number of nodes, the master nodes. The master nodes, shown in fig. 27, have been chosen according to what would have been necessary for the dynamic simulations:

- nodes that lie on the contact area;
- laser target points;
- clamped nodes;
- RP2 where the normal load F_n is applied;
- RP1 where the external periodic force F_{ex} is applied;

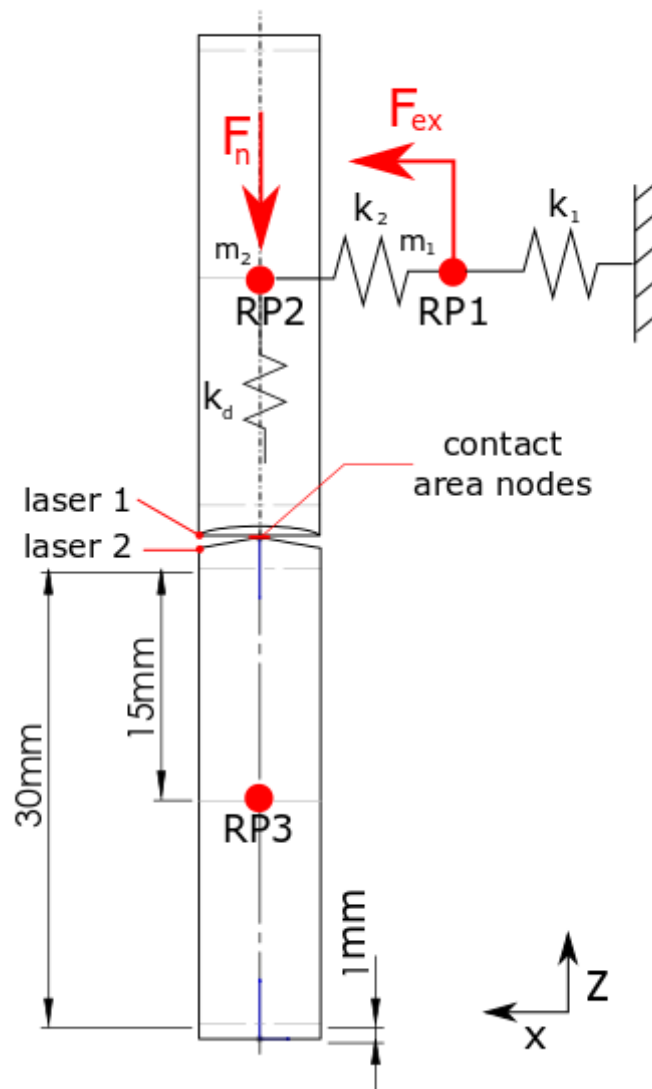


Figure 27: Master nodes

5.3 Code Interface

Once the modal shapes of the master nodes of each body have been evaluated, they have been recorded into two text files. The latter describe the dynamic behaviour of the two bodies as input for the code. The two text files have to be declared in the input file that will be read by FORSE. The input file has a specific format that can be subdivided in four main parts[6]:

- analysis controls;
- linear model definition ;
- non linear model definition;
- output requested.

All the input file parts examples given in the sections 5.3.1, 5.3.2 and 5.3.3 belong to the input file used to perform the dynamic simulations in this thesis.

5.3.1 Analysis controls

Analysis control data are responsible for control of the solution and tracing processes. These data have to be started with a line 'harmonic.balance' to indicate that input data required by the FORSE frequency-domain solver will follow. An example of the analysis controls data is shown in fig. 28. The meanings of each line are given in tab. 5.

```

*=====
* CONTROL DATA:
*=====

title test Test_Rig

harmonic.balance

start 0.05
end 3000
kHarm = 0 1 3 5 7 9
iHz = 0

p0 0
pk 1

*solvtype 1
tolerance 1e-06
*iArcCorrect 1
maxiter 10
ntrials 50

p1 0.01
p1min 0.0001  !*defines the step close to resonance
p1max 0.0005  !*defines the step far from resonance
cMin 0.8
cMax 0.99
sMin .1D-06
sMax .1D-00
iMin 3
iMax 7

nDOFnod = 3
idampcoef 0
idische 0
itrials -1

```

Figure 28: Example of analysis controls data

ANALYSIS CONTROLS	
KEYWORD	DESCRIPTION
start	analysis starting frequency
end	analysis ending frequency
Kharm	number of harmonics used in the multiharmonic expansion
lhz	Indicate unit for all frequencies: 1 – frequency is given in Hz, 0 – in rad/s. Default value is 1.
p0	Start value for the tracing parameter, default 0.0.
pk	End value for the tracing parameter
solvtype	Type of solver used for solution and tracing of nonlinear equations: 0 – Fried’s corrector 1 – Riks’s corrector (default value) 2 – Riks’s corrector for the reduced residual vector 3 – arclength corrector for full residual vector 4 – arclength corrector for reduced residual vector
tolerance	Error tolerance, default 10^{-6}
iArcCorrect	Indicates whether tracing parameter (and rotation speed) is fixed (=0) or not fixed (=1) at corrector phase of the solution process. Default value is 1.
MaxIter	Maximum number of iterations allowable for each step, default value is 100
ntrials	Coefficient of increase of the number of allowable iterations for search of a first, starting solution.
p1	Size of first step for tracing parameter, default 0.01
p1min	Minimum value for the tracing parameter step
p1max	Maximum value for the tracing parameter step

cMin	Minimum value for cosine between two consequential tangents to trajectory
cMax	Maximum value for cosine between two consequential tangents to trajectory
sMin	Minimum value for the step along trajectory of solutions
sMax	Maximum value for the step along trajectory of solutions
iMin	Minimum number of the iterations at each tracing step. This number is used as the primary criterion for automatic choice of the tracing parameter step. When this criterion is satisfied then cMin value is applied for tracing parameter variation.
iMax	Maximum number of the iterations at each tracing step. This number is used as the primary criterion for automatic choice of the tracing parameter step. When this criterion is satisfied then cMax value is applied for tracing parameter variation.
nDOFnod	is the number of the nodal degrees of freedom
idampcoef	Indicate meaning of coefficient used for description of modal damping
itrials	This is an optional parameter which allows choice of the initial approximation for solution used at the start of the analysis.

Table 5: Code controls data

5.3.2 Linear Model Definition

The linear part of the model has to be created and saved in a separate file. The name of the file, which can include a path to a necessary directory, has to be provided in the first line of input data for the linear model definition, shown in the example in fig. 29, recalling that the two specimens was named as body 1, the moving specimen on the top and body 2 the fixed specimen on the bottom as stated in section 4.2.

```

* =====
* model definition
* =====

model Body_1.mod
model Body_2.mod

* =====
* linear damping
* =====

modal.damping
      mode.data      1  0.001

* =====
* external forces
* =====

shaker cols
dof      amplitude      kharm      phase      scale
1 1      1              1          0.0       1.0

static cols
dof      amplitude
2 3      60

* =====
* non-linearity
* =====

graph cols
name      data
mu        0.88
kt        371.9008
kn        482.4710
cond      1
end graph

```

Figure 29: Example of linear model definition

LINEAR MODEL DEFINITION INPUT DATA		
KEYWORD	DATA PRESENTATION	DESCRIPTION
model	file name	Name of the file containing description of a major structure, modal model (has extension 'mod'), a generalised Guyan model (has extension 'mas')
modal.damping		Obligatory for a model provided by .mas file (Guyan model) and optional for model in .mod file (modal model)
mode.data	integer-real number	Damping factors for a specified mode

Table 6: Linear model definition input data

The shaker force element defines a periodic excitation force applied to a specific degree of freedom. The static force element defines where a static force is applied and its amplitude does not vary during the analysis. The two elements data are defined in tab. 7 and 8.

SHAKER ELEMENT DATA		
KEYWORD	DATA PRESENTATION	DESCRIPTION
dof	dof name	Define first DOF where the force is applied and direction: 1 x direction, 2 y direction, 3 z direction.
amplitude	real number	Amplitude of the force
kharm	integer number	Define the number of harmonics
phase	real number	Phase angle (degrees), default 0.0
scale	real number	Scale factor for amplitude, default 1.0

Table 7: Shaker element input data

STATIC ELEMENT DATA		
KEYWORD	DATA PRESENTATION	DESCRIPTION
dof	dof name	Define first DOF where the force is applied and direction: 1 x direction, 2 y direction, 3 z direction.
amplitude	real number	Amplitude of the force

Table 8: Static element input data

5.3.3 Non Linear Model Definition

Each pair of contact nodes (121) is linked by a non linear friction interface element fully described in section 5.1.1 . This element is characterised by specific mechanical properties:

- friction coefficient $\mu = 0.88$,
- tangential stiffness $k_t = 371.9008 \frac{N}{mm^2}$,
- normal stiffness $k_n = 1.3 \cdot k_t$ from literature,
- gap, normal distance between a pair of contact nodes.

The gap is variable depending on the contact nodes x and y coordinates. The gap varies because of the curvature of the contact interface and for each pair of nodes having the same x and y coordinates the normal distance has been calculated using the commercial software Matlab, fig. 30. The k_t value ($45000 \frac{N}{mm^2}$) has been evaluated experimentally, in particular looking at the steady state value. The latter has been divided by the number of nodes. E

f3pen cols							
nod1	nod2	kn	kt	mu	gap	cond	
7	206	kn	kt	mu	0.002899	cond	
8	221	kn	kt	mu	0.002899	cond	
9	319	kn	kt	mu	0.002041	cond	
10	230	kn	kt	mu	0.004997	cond	

Figure 30: Friction interface element definition

The voice "cond" in fig. 30 actually is an output request, the user can declare if he want as output the nodal condition for each frequency.

5.3.4 Output Requested

The aim of the dynamic simulations in this thesis is to get the harmonic expansion of the displacements of the target points of the two lasers and the harmonic expansion of the tangential force linked to each contact node building up during the sliding motion. The relation between the difference of the lasers point displacements and the overall tangential forces gives the hysteresis loop in unworn condition. The hysteresis loop is evaluated in one cycle period

according to $T = \frac{1}{f}$ where f is around 100 Hz since in the experimental tests the frequency of the periodic external force F_{ex} is 100 Hz. The output requested are shown in fig. 31 .

```
output
i3Damp1 = 0
displ 128 1
! force 1 1
displ 321 1
force 7 1
```

Figure 31: Outputs requested

OUTPUTS		
KEYWORD	DATA PRESENTATION	DESCRIPTION
i3Damp1	1-0	Indicates whether the maximum displacement in three-dimensional motion (=1) or the maximum displacement for a single specified DOF (=0)
displ	dof name integer number	number of nodes to be analysed and direction, 1 is for x tangential direction
force	dof name integer number	number of nodes to be analysed and direction, 1 is for x tangential direction

Table 9: Output definition

5.4 Numerical Results

The simulations was performed with 5 odd harmonics as generally done in studies [2]. The input parameters for the simulations were:

- friction coefficient $\mu = 0.88$;

- fixed normal load F_n : 60 N;
- different external forces F_{ex} : 1,10,30,50,70,90 N

The different amplitudes of external forces lead to different contact area conditions, stick, slip, full contact or combination of the three . All these conditions have an effect on the frequency response, as shown in fig.32 where the nodal condition have been evaluated for the two resonance peaks at 38.9 Hz for a full sliding condition and 400 Hz where the most of the nodes in contact are in stick condition. Above 400 Hz the FRFs are interrupted because the main mode of interest is the first one, which varies between 40 and 400Hz

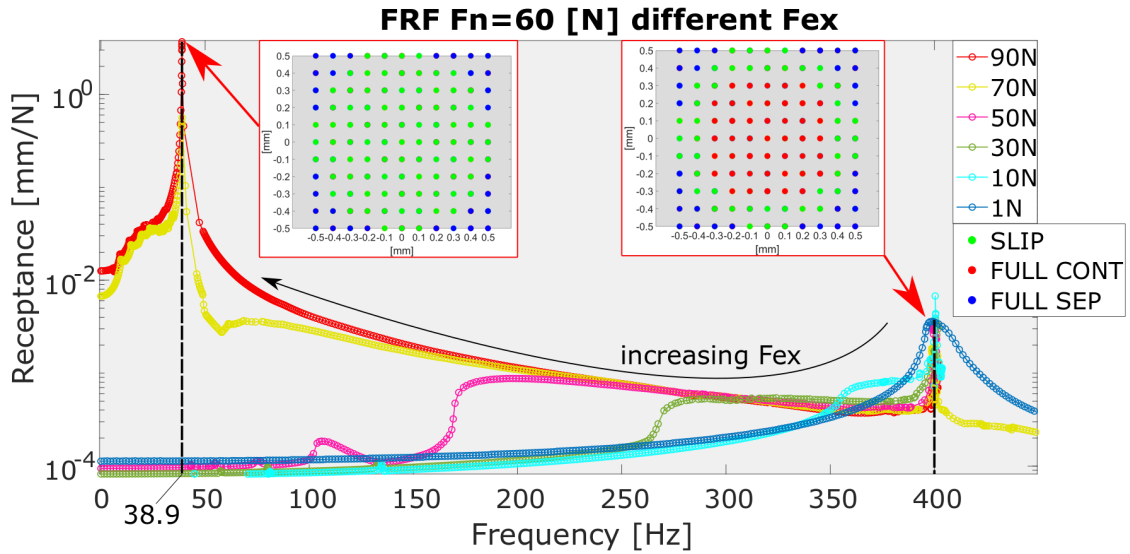


Figure 32: Forced response

The frequency taken into account to analyse the tangential contact stiffness K_t is the one used for the experimental measurements, 100 Hz. At this frequency the harmonic expansion of the displacements of the two laser points and the harmonic expansion of the nodal tangential force have been obtained in order to pass from the frequency domain to the time domain. The relation between the difference of the two displacement and the total tangential force gives the hysteresis loops for different external excitation forces. The precision of the results depends on the number of harmonics, but higher is the number of harmonics taken into account, higher would be the computational time as stated in section 5.1. The K_t analysis was performed with

15 odd harmonics because for very large sliding conditions the hysteresis loops need a larger number of harmonics to be better captured as shown in fig. 33 .

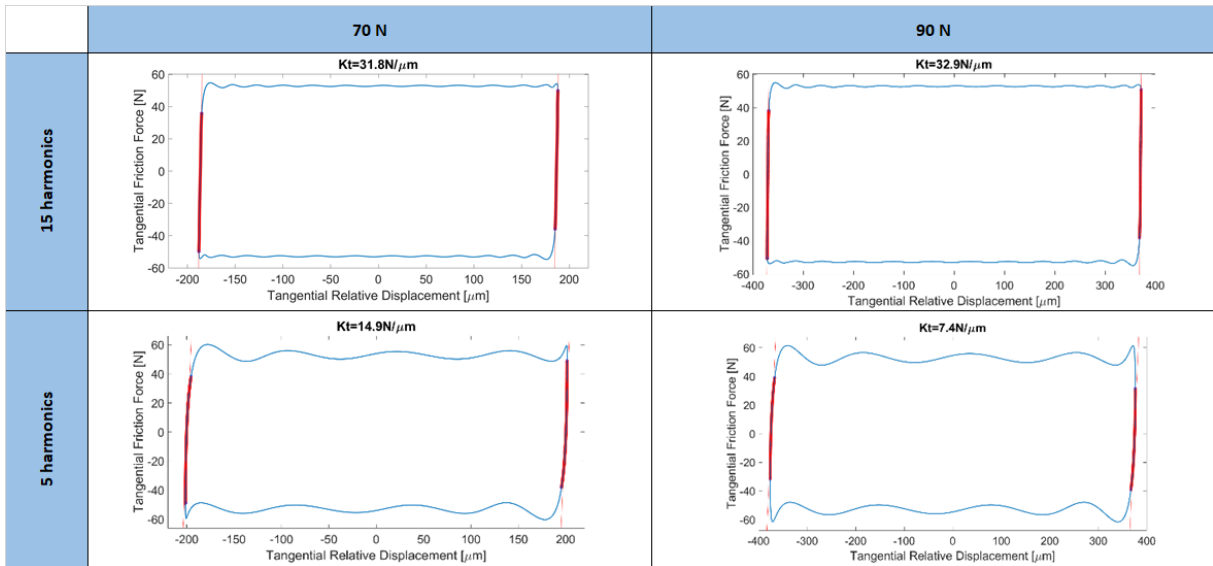


Figure 33: Comparison of the hysteresis loops for 5 and 15 odd harmonics

The number of harmonics chosen is 15 due to computational limits. The harmonic expansions of the total tangential force, the lasers displacements and the hysteresis loops are shown in fig. 34.

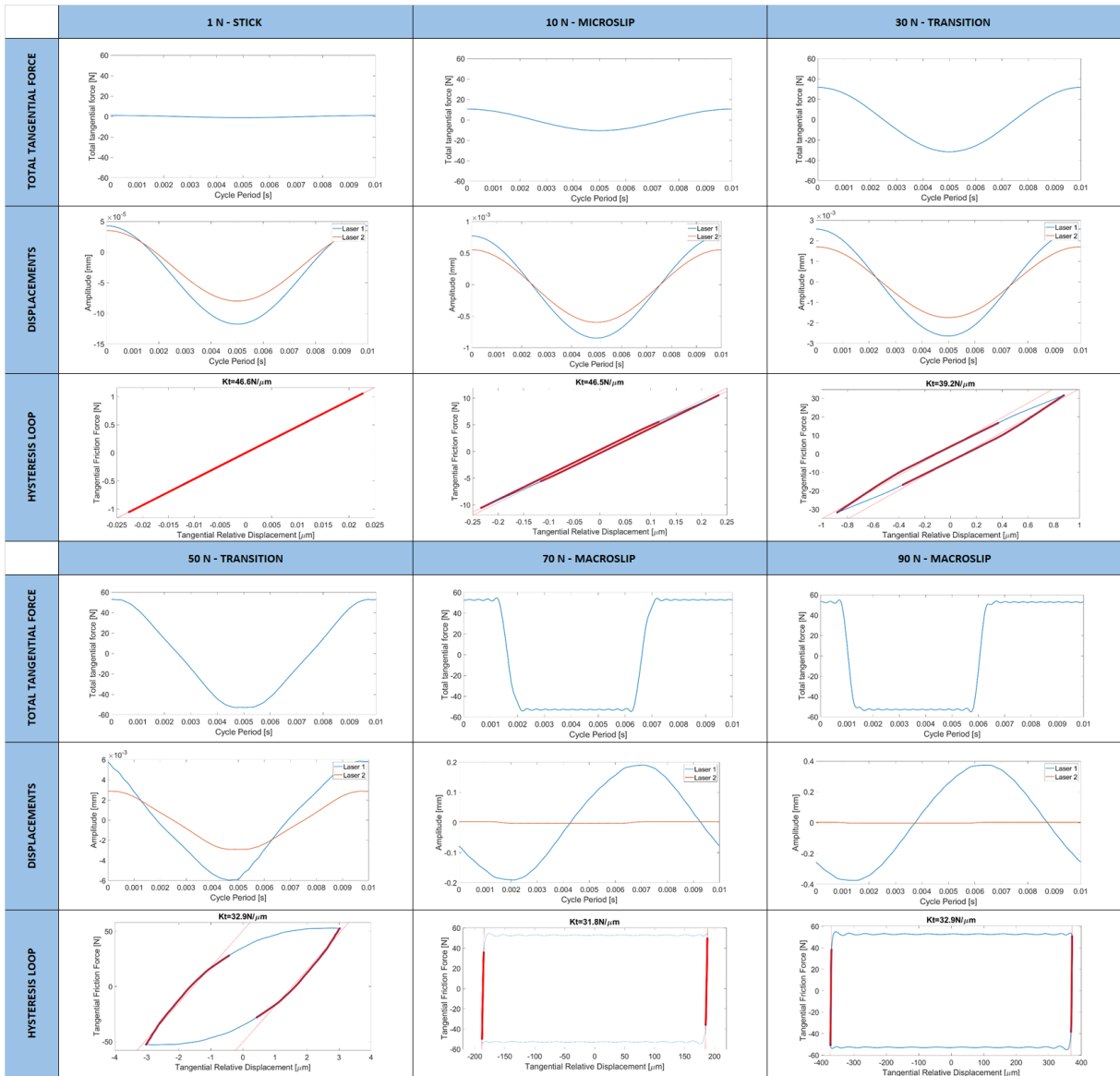


Figure 34: From harmonic expansions to hysteresis loops

Looking at fig. 34 the k_t seems to decrease increasing the external force amplitude. A further analysis has been conducted in order to verify if the k_t decreases or not. In particular the stick portion of the hysteresis loops has been compared as shown in fig 35.

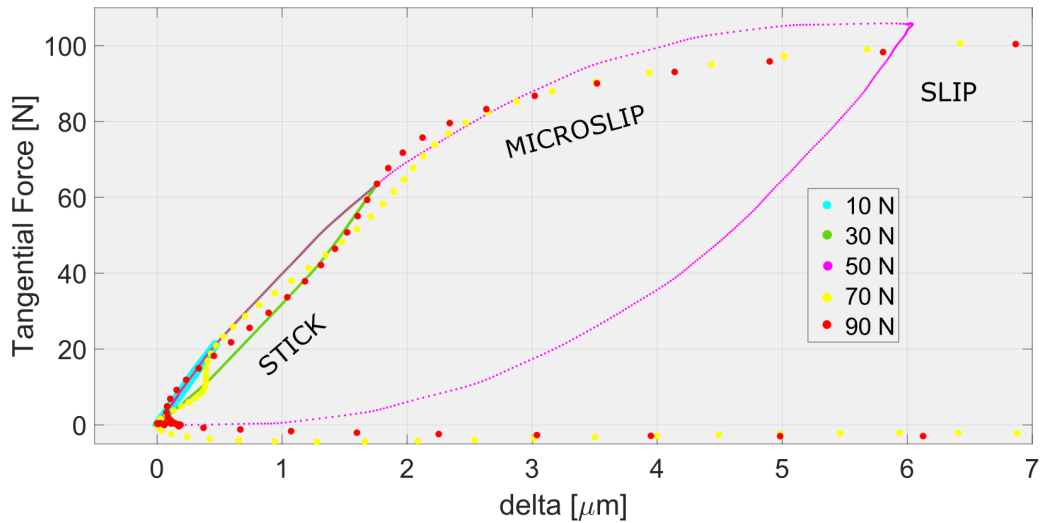


Figure 35: Stick portions comparison

It is clear looking at the fig. 35 that the stick portions of the 10, 30, 50 N external force cases have the same slope, for the other two cases the stick portion is not well defined yet and if an higher number of harmonics was used the k_t would be the same of the other cases. Increasing the external force the sliding increases and so the energy dissipation, represented by the hysteresis loop area. The energy dissipation is directly related to the magnitude of the external force, changing the dynamic behaviour of the entire system. This concept is validate experimentally.

5.5 Experimental Results and Comparison

The aim of the experimental tests [8] in this section is to analyse the dynamic response of the friction rig to the hysteresis loop variations at the contact interface. The hysteresis loops were measured for different normal load under a 100 Hz periodic excitation. After the evaluation of the hysteresis loops an hammer test has been performed in order to get the test rig dynamic behaviour. Hammer tests were conducted with hammer impacts of 100 N and the response was measured with an accelerometer placed on the moving arm. The evolution of the experimental measured FRFs is shown in fig.36.

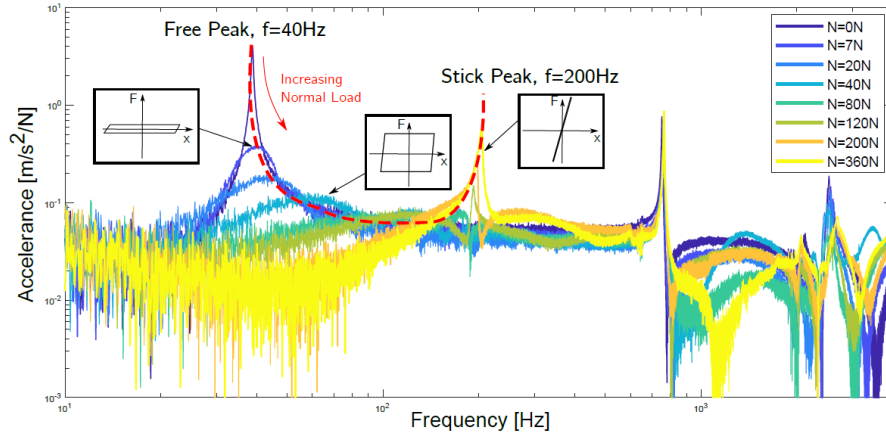


Figure 36: Experimental FRFS [8]

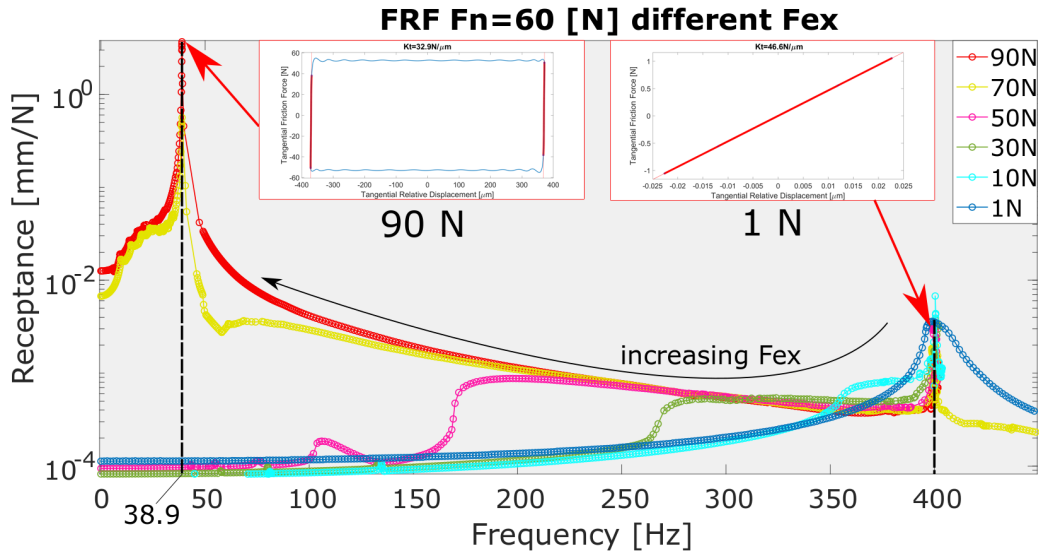


Figure 37: Numerical FRFs

In particular the experimental results in fig. 36 must be compared to the numerical results in fig. 37. The difference is that for numerical results the amplitude of the periodic external force varies instead the normal load is the same. For what concern the experimental results the first mode moves from 40 Hz at very low normal loads to 200 Hz at very high normal loads. For what concern the numerical model the resonance peak moves from 400 Hz for very low external force, to 38.9 Hz for high external force. Low external force means poor sliding, in fact as shown in fig.32 a stick condition is established. High external force means more sliding and a

sliding condition is established. The increase in the sliding distance results in wider hysteresis loops that lower the overall stiffness of the joint, and hence lower the natural frequency of the system [8], those leading to have the same effects of the experimental measurements on the numerical simulations.

6 Conclusions and Discussions

Quasi-static simulations and dynamic simulations have been performed in this thesis to replicate the fretting experimental results obtained from the test rig of the Imperial College of London [1] [8]. The quasi-static simulations have been performed using a numerical wear code based on the Finite Element method developed in Politecnico di Torino [3], while the dynamic simulations have been performed using a multi-harmonic balance method based numerical code developed in Imperial College of London [2] [7]. The aim of the quasi-static simulations was to obtain the evolution of the tangential contact stiffness with wear for different normal loads and compare it with the experimental results. The aim of the dynamic simulations was to obtain the response functions for different excitations and compare them with the experimental ones. In addition the hysteresis loops were also obtained from simulations, from which the contact stiffness was evaluated. Results highlighted some interesting features on the used numerical methods.

In particular from the quasi-static simulations highlighted that:

- The numerical code is capable of accurately capturing the evolution of the contact stiffness observed in the experiment, given that a realistic finite element model is used as input in the simulations. In fact, the initial FE model used in simulations could not capture the experimental trends, and it had to be updated to better approximate the real morphology of the friction rig fretting specimens.
- The numerical values of the contact stiffness were two times larger than the experimental ones. This deviation in the values could be attributed to the numerical assumption of a perfectly smooth contact, whereas in reality the stiffness is reduced due to micro scale roughness at the contact.
- The contact stiffness in the numerical results grows with wear because the contact area increases with the energy dissipated until a uniform pressure distribution is reached. When a uniform pressure is reached, the contact stiffness becomes constant and reaches a steady state condition. This is the same trend observed in experiment. However the numerical steady state value do not seem to depend on the normal load on the contrary

of what observed in the experimental tests.

For what concern the dynamic simulations, the results have shown that:

- The MHBM numerical code is able to correctly capture the evolution of the FRFs that is observed in the experiments. In addition, for every FRF, hysteresis loops and contact conditions were computed and compared with experiments, showing a good agreement in the trends.
- In particular , the FRFs obtained for different excitation forces show that the first resonance moves from stick peak at 400 Hz to a free peak at 39 Hz as shown in the experimental results. This confirms that the model used in simulations is reliable.
- A sensitivity analysis on the number of harmonics has been performed and it has been shown that the number of harmonics chosen to fit the tangential displacement and the tangential force, strongly affect the precision of the resultant hysteresis loops and as a consequence affect the contact stiffness values. The contact stiffness values are evaluated using 5 odd harmonics and 15 odd harmonics. The comparison between the two cases shows that for stick or transition conditions the values are similar but if the slip condition occurs 5 odd harmonics are no more sufficient to get the contact stiffness value with precision. In addition, it was found that the tangential contact stiffness depends on the amplitude sliding, even this dependency might just be due to a wrong approximation due to the insufficient number of harmonics used for the simulations.

Concluding, this thesis has shown that the two modelling approaches were capable to replicate the trends observed in experiments, and the discrepancies in the final values were justified by the underlying assumptions of the models. In the future, more simulations can be conducted by using numerical models more similar to the real structures, on the way to be able to replicate the behaviour of complex structures with frictional contacts.

References

- [1] A. Fantetti, L. R. Tamatam, M. Volvert, I. Lawal, L. Liu, L. Salles, M. R. W. Brake, C. W. Schwingshackl, D. Nowell. “The Impact of Fretting Wear on Structural Dynamics: Experiment and Simulation”. In: (2019).
- [2] Armand, J., Pesaresi, L. , Salles, L. , Schwingshackl, C. “A Multiscale Approach for Non-linear Dynamic Response Predictions With Fretting Wear,” in: *Journal of Engineering for Gas Turbines and Power* 139 (2017).
- [3] D. Botto and M. Lavella. “A numerical method to solve the normal and tangential contact problem of elastic bodies”. In: *Wear* 330-331 (2015), pp. 629–635.
- [4] C.M. Firrone, S. Zucca. “Modelling Friction Contacts in Structural Dynamics and its Application to Turbine Bladed Disks,” in: *Numerical Analysis - Theory and Application* (2011).
- [5] M.J. Starr D.J. Segalman. “Inversion of Masing models via continuous Iwan systems”. In: *Non-Linear Mech.* 43 (2008), pp. 74–80.
- [6] E.P. Petrov. “FORSE manual”. In: (London, 2010).
- [7] E. Petrov, D.J. Ewins. “Analytical Formulation of Friction Interface Elements for Analysis of Nonlinear Multi-Harmonic Vibrations of Bladed Disks,” in: *Journal of Turbomachinery* 125 (2003), pp. 364–371. DOI: 10.1115/1.1539868.
- [8] Fantetti, A., Schwingshackl, C. “EFFECT OF FRICTION ON THE STRUCTURAL DYNAMICS OF BUILT-UP STRUCTURES: AN EXPERIMENTAL STUDY”. In: *Turbomachinery Technical Conference and Exposition* (London, 2020).
- [9] G. Genta. “Vibration Dynamics and Controls”. In: Springer, 2009. Chap. 15.
- [10] H. Hertz, “Über die Berührung fester elastischer Körper,,” in: *Jnl. reine und angewandte Mathematik* 92 (1882).
- [11] D. A. Hills M. Ciavarella and G. Monno. “The influence of rounded edges on indentation by a flat punch,” in: *Proc. Inst. Mech. Eng. Part C J Mech. Eng. Sci.* 212.4 (1998), pp. 319–327.

- [12] M. H. Müser, W. B. Dapp, R. Bugnicourt, et al., “Meeting the Contact-Mechanics Challenge,” in: *Tribology Letters* 65.4 (2017).
- [13] Schwingshackl, C., Petrov, E., and Ewins, D. “Measured and Estimated Friction Interface Parameters in a Nonlinear Dynamic Analysis,” in: *Mech. Syst. Signal Process.* 28 (2012), pp. 574–584.
- [14] C.W. Schwingshackl. “Measurement of Friction Contact Parameters for Nonlinear Dynamic Analysis”. In: (2012).

List of Figures

1	Typical hysteresis loop	5
2	Cylindrical specimens	13
3	Test rig [14]	14
4	Flow chart of the procedure to solve the normal contact problem [3]	18
5	Flow chart of the procedure to solve the tangential contact problem [3]	19
6	Example of virgin curve [3]	20
7	main dimensions of the specimen in mm	21
8	specimens 3D models	22
9	brick element with relative nodes	23
10	comparison between modelled and real specimen	23
11	double curvature highlight	24
12	Specimen clamping	25
13	Comparison between the full model and the reduced one	26
14	Matrix non zero elements	26
15	FEM specimens assembly	28
16	Flat contact area cycle conditions for 17 N normal load case	31
17	Kt versus number of cycles (Flat case)	32
18	Contact area conditions for different number of cycles, 17 N normal load (Curved case)	33
19	Kt versus number of cycles (Curved case)	34

20	Kt versus cumulative energy dissipated	35
21	Experimental results	36
22	Computational flow chart [2]	39
23	Interface element [7]	40
24	2DOF lumped parameters model [8]	42
25	Complete system [1]	43
26	Implementation of the 2DOF model	44
27	Master nodes	45
28	Example of analysis controls data	47
29	Example of linear model definition	50
30	Friction interface element definition	53
31	Outputs requested	54
32	Forced response	55
33	Comparison of the hysteresis loops for 5 and 15 odd harmonics	56
34	From harmonic expansions to hysteresis loops	57
35	Stick portions comparison	58
36	Experimental FRFS [8]	59
37	Numerical FRFs	59

List of Tables

1	Frequencies for each model	27
2	Code inputs matrices	29
3	Code simulations parameters	29
4	Outputs requested	30
5	Code controls data	49
6	Linear model definition input data	51
7	Shaker element input data	52
8	Static element input data	52
9	Output definition	54